RFO1, a novel pectin-integrity receptor with dual functionality in development and defense

Apolonio I. Huerta[1], Juan Carlos Montesinos[1], Gloria Sancho-Andrés[1], Javier Silva-Navas[2], Christopher Kesten[1,3], Rudolf Schlechter[1,4], Temurkhan Ayupov[1,5], Julia Santiago[2], Clara Sánchez-Rodríguez[1*]

[1]ETH Zurich, Institute of Molecular Plant Biology (D-BIOL) - Zurich, Switzerland.
[2]University of Lausanne, Department of Plant Molecular Biology - Lausanne, Switzerland.
[3]Ender diagnostics AG,ESL-INV Industriestrasse 30, 8302 Kloten, Switzerland
[3]Current address: Lonza AG, Visp, Switzerland.
[4]Current address: Institute of Microbiology, Freie Universität Berlin, Berlin, Germany
[5]Current address: Institute of Molecular and Clinical Ophthalmology - Basel, Switzerland.

[*]Corresponding author: clara_sanchez@ethz.ch

MAIN TEXT

Highlights

- RFO1 is the first WAKL identified as a sensor of demethylated pectin at the cell wall.
- RFO1 mediates plant responses to altered pectin methylation levels at the cell wall caused by *Fusarium oxysporum* infection.
- RFO1 is a novel positive regulator of BR signaling required for normal growth under conditions of altered PME activity.

Summary

All organisms adjust their development according to their environmental conditions. For most, this implies sensing the alterations caused to their cell walls (CWs) by different cues. Despite the relevance of this process, few molecular players involved in CW-sensing are known and characterized. Here, we show that the wall-associated kinase-like receptor RESISTANCE TO FUSARIUM OXYSPORUM 1 (RFO1) is required for plant growth and early defense to Fo by sensing changes in the pectin-methylation levels at the CW. RFO1 dwell time at the plasma membrane is affected by that CW pectin-methylation-status, regulating MITOGEN ACTIVATED PROTEIN KINASE and gene expression pathways. We demonstrate that the extracellular domain of RFO1 binds de-methylated pectin, whose distribution at the CW is altered during Fo infection. Furthermore, we show that RFO1 is required for the BR-dependent plant growth alteration in response to inhibition of pectin de-methyl-esterification at the CW. Our study demonstrates that RFO1 is a novel pectin sensor that plays a unique dual role in plant growth and defense against vascular pathogens.

Introduction

Most cells have a wall as their outermost layer surrounding, and connected with, their plasma membranes (PMs). The cell wall (CW) allows cell expansion while preventing its rupture. Thus, the wall is indispensable for the survival of its cell and, in multicellular organisms, permits cell adhesion. The main properties of CWs i.e. strength and extensibility, rely on chemical interactions among the polysaccharides that build their core structure, as well as the capacity to rearrange these constituents rapidly at a subcellular level (Bidhendi and Geitmann, 2016)). This is particularly relevant for plants that need to adjust their development to a constantly changing environment (Vaahtera et al., 2019).

The plant CW core is composed of the polysaccharides cellulose, hemicelluloses and pectins. As the most hydrophilic and flexible CW polysaccharide, pectins have a central role in plant growth and acclimation to the environment. Pectins have a homogalacturonan (HG) back-bone that makes them structurally significantly different from the β-1,4-Glc-based cellulose and hemicellulose polysaccharides (Albersheim et al., 1996; Mohnen, 2008). The pectin polygalacturonic acid core is secreted heavily decorated with methyl and/or acetyl groups (Anderson, 2016; Mohnen, 2008). Once at the CW, extracellular enzymes called PECTIN METHYLESTERASES (PMEs) and PECTIN ACETYLESTERASES gradually remove those decorations, while PME inhibitors (PMEIs) counter the action of PMEs by direct inhibition of their catalytic domains (Wormit and Usadel, 2018). These changes in pectin decorations modify the physicochemical properties and, consequently, the structure and function of the

CW. Therefore, perturbing the delicate balance between methyl- and demethylated pectin (mPectin and dmPectin, hereafter) has severe consequences for plant growth and defense (Engelsdorf et al., 2018; Fan et al., 2017; Feng et al., 2018; Liu et al., 2018; Wolf et al., 2012). These developmental responses to pectin alterations start with cellular monitoring of the state of its CW through PM-localized receptors, among other sensors (Ringli, 2010). In the context of plant growth, the Arabidopsis PM-localized receptor kinase FERONIA has recently been shown to regulate pavement cell morphogenesis upon binding to highly dmPectin (Lin et al., 2021). In Arabidopsis, the PM-receptors BRI1 (BRASSINOSTEROID INSENSITIVE 1) and RLP44 (RECEPTOR-LIKE PROTEIN 44), together with the BRI1 co-receptor BAK1 (BRI1 Associated Kinase 1), have been reported to coordinately mediate plant responses to abnormally high levels of mPectin present at the CW (Glöckner et al., 2020; Wolf et al., 2012, 2014). Similarly, the WALL ASSOCIATED KINASEs (WAKs) and WAK-likes (WAKLs), participate in controlling cell expansion (Lally et al., 2001; Li et al., 2021; Wagner and Kohorn, 2001; Wu et al., 2020), presumably by sensing pectin perturbations. Indeed, WAK1 and WAK2 were reported to bind and respond to dmPectin but not highly mPectin (Anderson et al., 2001; Decreux et al., 2006; He et al., 1996; Kohorn et al., 2009).

WAKs have also been shown to function as sensors of pectin oligomers, named oligogalacturonides (OGs), released upon wounding and pathogen infection (Brutus et al., 2010). Additionally, transcriptomic data indicate that most WAKs and WAKLs are important for plant defense (Ferrari et al., 2013; Menna et al., 2021). This function is demonstrated by a high and increasing number of reports in different crops, including wheat (Dmochowska-Boguta et al., 2020; Saintenac et al., 2018), cotton (Wang et al., 2020; Yang et al., 2021), and tomato (Rosli et al., 2013). Although WAKLs contain similar extracellular domains as to those present in WAKs, their association with the plant CW has not been previously demonstrated (Verica and He, 2002; Verica et al., 2003). In addition, recent studies in cotton and tomato suggest that the role of WAKs and WAKLs in signal transduction expand beyond that of responding to pectin changes (Qi et al., 2021; Wang et al., 2020; Zhang et al., 2020). The cotton GhWAK7A seems to be needed for chitin but not OGs perception during infection with vascular fungi (Wang et al., 2020). The tomato TaWAK7D, required for defense against a necrotrophic fungus, appears to participate in plant responses to both chitin and pectin (Qi et al., 2021). In addition, WAK1 and other members of the family are suggested to participate in flagellin-triggered immunity (Zhang et al., 2020). Among the WAKs and WAKLs identified to play a role in Arabidopsis responses towards pathogens, WAKL22 was found to be required for resistance to *Fusarium oxysporum* (Fo) and *Verticillium sps.* wilts and therefore named RFO1 (RESISTANCE TO FUSARIUM OXYSPORUM 1) (Diener and Ausubel, 2005; Verica and He, 2002).

Root vascular fungi like Fo and Verticillium are among the most detrimental pathogens worldwide affecting high-value crops and plants in natural ecosystems (Gordon, 2017; Klosterman et al., 2009). Fo and Verticillium infection begins at the epidermis and progresses to the xylem mainly intercellularly; i.e., through the apoplast. Once in the root vasculature, the fungi proliferate, blocking the xylem and causing wilting and, ultimately, plant death (Bishop and Cooper, 1983). In its path towards the root vasculature, Fo and Verticillium modify and degrade the plant CWs, through the secretion of a wide range of CW modifying enzymes (Bravo-Ruiz et al., 2017; Glass et al., 2013; Jonkers and Rep, 2009), including PMEs, pectin and pectate lyases, and polygalacturonases (Bravo Ruiz et al., 2016; Cooper and Wood, 1975; Di Pietro and Roncero, 1998; Durrands and Cooper, 1988; Fan et al., 2017; Gámez-Arjona et

al., 2021; García-Maceira et al., 2000; García-Maceira and Di Pietro, 2001; Huertas-González et al., 1999; Safran et al., 2021; Wojtasik et al., 2011; Yang et al., 2018). It is vital for a host plant's survival to sense these pectin modifications, either directly or through the sensing of pectin degradation products, as part of their response to these root vascular pathogens and mediate growth-defense processes. However, no PM-localized receptor has been identified to play this vital function. To fill this gap in knowledge, we characterized the role of RFO1 as a putative sensor of the pectin methyl esterase status at the CW. Here, we link RFO's function to the detection of altered pectin methylation at the CW produced during Fo infection and generated by PME inhibition. The results presented here demonstrate that RFO1 has a dual role in pectin sensing during both plant development and defense.

Results

RFO1 is a PM-localized receptor necessary for root resistance to *Fusarium oxysporum*. To evaluate the role of RFO1 in plant defense against Fo in the root, we characterize the infection phenotype of the mutant *rfo1-1* following a previously described plate infection assay employing Fo5176 pSIX1::GFP (Kesten et al., 2019; Huerta et al., 2020). While there were no growth differences between wild type control, Col-0 (WT) and *rfo1-1* under mock condition, the mutant showed less root growth inhibition during the first days of the interaction (0-3 days post transfer to plates containing Fo microconidia) than WT. (Fig. 1A,B and S1A,B). Additionally, *rfo1-1* plants showed increased vascular colonization compared to WT, starting at 4 dpt (Fig. 1C). To confirm RFO1 function in plant response to root-colonization by Fo, we complemented *rfo1-1* plants with a C-terminal tagged GFP fusion driven by its promoter (*pRFO1::RFO1-GFP*). The resulting RFO1-GFP complemented line showed no altered phenotypes compared to *rfo1-1* and WT plants (Fig. S1A and B), but the *rfo1-1* susceptibility phenotype was restored to WT (Fig. 1D), confirming the functionality of the complemented line. In addition, the expression of *RFO1* increased two times in Fo-infected WT roots at 2, 3, 5 and 6 dpt (Fig. 1D). Our results suggest that *rfo1-1* susceptibility to Fo might be a consequence of RFO1's role in root resistance to Fo before the fungus reaches the vasculature. Increased RFO1 levels seem to be required by the plant to slow-down the entrance of Fo in the xylem, inducing growth-defense tradeoffs.

To characterize the *in vivo* transcriptional activation of *RFO1*, plants were generated expressing RFP fused to a C-terminal N7-nuclear localization signal under the control of the *RFO1* promoter (*pRFO1::RFP-N7*). Expression of RFP-N7 was observed in, but was not limited to,root epidermal cells in mock-treated roots and roots exposed to Fo5176 pSIX1::GFP microconidia and imaged after one day (Kesten et al., 2019; Huerta et al., 2020) (Fig. S1C and D). The nuclear-localized RFP signal was significantly enhanced in root epidermal cells of the root tip exposed to Fo5176 pSIX1::GFP pre-germinated microconidia, compared to mock (95.4 ± 8.2 a.u. for mock *vs* 110.0 ± 23.3 a.u. for Fo5176). These results suggest that there is increased *RFO1* expression upon Fo infection, corroborating the results obtained by qPCR (Figure 1D).

The localization of RFO1 at the PM was confirmed through optical longitudinal cross-sections of RFO1-GFP root cells stained with the fluorescent lipophilic dye FM4-64 (Miyake and McNeil, 1995). Composite overlays of these sections demonstrated that RFO1-GFP and FM4-64 signals co-localize at the PM (Fig. 1E). Spinning disk confocal microscopy followed by single-particle tracking showed that RFO1-GFP is organized in discrete foci at the PM with an

average dwell time of 4.89 s (Fig. 1F and G, Fig. S1C, Movie S1). These RFO1 foci exhibit dynamics characteristic of free diffusion, as demonstrated by the linear fit of particle mean squared displacement (MSD) plots (Fig. S1D). Our results confirm the predicted localization of RFO1 at the PM and describe its particle dynamics.

RFO1 is required for plant growth responses to perturbation of pectin methylation at the cell wall

Extracellular GUB and EGF domains found in WAKs and WAKLs, including RFO1 (Fig. S2A), have been implicated in WAK perception of dmPectin (He et al., 1996; Wagner and Kohorn, 2001)**.** To determine if RFO1 can mediate plant response to perturbations in pectin methylation, plants were treated with epigallocatechin gallate (EGCG), a pharmacological inhibitor of PMEs at the CW (Lewis et al., 2008). EGCG treatment induces root growth inhibition in Arabidopsis seedlings, presumably through its role in decreasing the levels of dmPectin at the CW (Lewis et al., 2008). *rfo1-1* seedlings showed significantly decreased root growth inhibition upon EGCG treatment compared to WT and RFO1-GFP plants (Fig. 2A and B), suggesting that RFO1 is required for plant responses to EGCG. To ensure that the decreased *rfo1-1* sensitivity to EGCG was due to PME inhibition and not to any off-target effects of the drug, *rfo1-1* was introduced into the PMEIox mutant background (Wolf et al., 2012) which over-expresses *PMEI5*. This overexpression of *PMEI5* activity at the CW increases the levels of mPectin. The resulting *rfo1-1* PMEIox plants were phenotypically indistinguishable from WT, indicating that *rfo1-1* suppressed *PMEI5* overexpression phenotypes (Fig. 2C and D). In addition, when RFO1-GFP was introduced in the *rfo1-1* PMEIox background, the PMEIOx-induced pectin perturbation phenotypes were restored (Fig. 2C and D). Altogether, these data indicate that RFO1 is required for mediating plant responses to chemical or genetic perturbation of pectin methylation at the CW.

The extracellular domain of RFO1 in Col-0 plants is necessary for the defense against Fo and for detecting alterations in the pectin methylation status

Previous studies demonstrated that the Arabidopsis Ty-0 ecotype variant of RFO1 ($RFO1^{Ty\text{-}0}$) is impaired in its ability to confer resistance against *F. oxysporum* (Diener et al 2005). Using our plant infection assay, we confirmed this observation at the root level using $RFO1^{Ty\text{-}0}$-GFP (*rfo1-1* $RFO1^{Ty\text{-}0}$-GFP) plants (Fig. S2B). In addition, $RFO^{Ty\text{-}0}$-GFP plants are less sensitive than WT to the root inhibition induced by EGCG (Fig. S2C and D), and do not suffer from PMEIox growth defects when in the *rfo1-1 PMEIox* background (Fig. S2E), resembling in both cases to *rfo1-1* mutant. These results suggest that $RFO^{Ty\text{-}0}$ is not involved in plant resistance against Fo in the root and is also not required for sensingaltered pectin methylation status at the CW (Fig. S2C and D).

To understand which part of the $RFO1^{Col\text{-}0}$ is essential for pectin integrity sensing and defense against Fo, we generated a chimeric RFO1 receptor through the fusion of the extracellular (ec) and the transmembrane domain of $RFO1^{Col\text{-}0}$ and cytosolic domain (kt) of $RFO1^{Ty\text{-}0}$. The resulting chimera was driven by the $RFO1^{Col\text{-}0}$ promoter (pRFO1::$RFO1^{eckt}$-GFP) and was expressed in a *rfo1-1* background ($RFO1^{eckt}$-GFP). The $RFO1^{eckt}$-GFP chimera was found to be localized at the PM of root epidermal cells, where it is organized as foci similar to $RFO1^{Col\text{-}0}$-GFP and $RFO1^{Ty\text{-}0}$-GFP particles (Fig. S2F). Furthermore, $RFO1^{eckt}$-GFP roots did not show growth alterations (Fig. S2G). $RFO1^{eckt}$-GFP could restore *rfo1-1* susceptibility to Fo5176 to WT levels, as observed in $RFO1^{Col\text{-}0}$-GFP plants (Fig. 3A). In addition, the F1 *rfo1-1* (-/-) $RFO1^{eckt}$-GFP (+/-) PMEIox (+/-) plants were phenotypically indistinguishable from PMEIox

and *rfo1-1* RFO1^{Col-0}-GFP PMEIox (Fig. 3B), indicating that the extracellular domain of RFO1^{Col-0} is important to perceive the pectin modifications caused by *PMEI5* overexpression (Fig. 3B). Contrary to that observed in RFO1^{Ty-0}-GFP, the chimera variant shows similar sensitivity to EGCG than RFO1^{Col-0}-GFP(Fig. 3C and S2B-C). These data suggest that the RFO1^{Col-0} ectodomain is sufficient for maintaining RFO1 functionality in defense against Fo5176 pSIX1::GFP and for plant response to modifications in the pectin methylation status at the CW.

The RFO1 ectodomain binds to demethylated pectin

To test the role of the extracellular domain of RFO1 in plant response to different levels pectin methylation, we performed dot immunobinding assays. We produced dmPectin from apple-derived mPectin and immobilized both of them on nitrocellulose membranes that were exposed to either recombinant C-terminal SNAP-tagged extracellular domain of RFO1 (RFO1^{ECD}) or recombinant SNAP tag, as a negative binding control (Fig. S3 and S4A). The immunoassays demonstrated *in vitro* binding of RFO1^{ECD} to dmPectin but not to mPectin, while little to no binding was observed when using the SNAP alone (Fig. 3D and E). Both RFO1^{ECD}-SNAP and SNAP bound plant CW glycoprotein extracts (GP; Fig. S4A), demonstrating that the SNAP control protein allows to differentiate specific (dmPectin, Fig. 3D and E) from non-specific (GP, Fig. S4A) *in vitro* binding to CW components. These results suggest that RFO1 might act as a sensor of dmPectin.

To clarify the role of RFO1 during plant defense against Fo5176, the pectin methylation status of mock and Fo5176-infected roots at 3 dpt was examined in the three CW soluble fractions. This fractionation method removes soluble polysaccharides based on the strength of their attachment to other CW components, starting with the removal of loosely associated pectins (fraction I), and ending with hemicelluloses and pectins covalently-linked to the insoluble cellulose (fraction III) (Hotchkiss and Hicks, 1990; Mort et al., 1991). The obtained fractions were consequently immobilized onto nitrocellulose membranes and probed with antibodies against CW-derived dmPectin (JIM5; (Casero and Knox, 1995)) and mPectin (JIM7; (Knox et al., 1990)). JIM5 binding decreased in fraction I and III, while increased in fraction II of infected roots compared to mock samples (Fig. 3F and G, Fig. S4B and Fig. S4C). No differences were observed in the capacity of JIM7 to bind the different fractions in mock or fungal-infected roots. As fraction III is extracted using a dilute base which removes all pectin methyl groups, the reduction in JIM5 probing and the absence of JIM7 binding to this fraction might be a result of a reduction in total pectin (Fig. S4B and Fig. S4C). Our data indicate that Fo5176 infection specifically modifies the levels of dmPectins found in fraction I and II while leaving the levels of mPectin mostly unaffected.

Further dot immunobinding assays were performed to determine if RFO1^{ECD} binds to CW fractions in a dmPectin-dependent manner, using CW fractions obtained from mock and Fo5176-infected roots. The CWs of *in vitro* grown Fo5176 hyphae were fractionated in a similar way as root CWs and included as negative control. RFO1^{ECD} binding to the immobilized CW fractions correlated with the changes observed in dmPectin levels within fraction I and II after Fo5176 infection, determined by the previous JIM5/JIM7 immunobinding assays (Fig. 3H and I). The fraction III was not included in the assay as it does not help to differentiate the pectin methylation state level (Fig. S4B and S4C). The SNAP negative control showed no differential pattern of binding to dmPectin within CW fractions (Fig. S4D). Together, these data indicate that levels of dmPectin in root CW fractions are altered during Fo infection, and RFO1 acts in sensing these modifications through differential binding to dmPectin.

RFO1 triggers MAPKs signaling and gene expression activation in response to altered dmPectin levels

Phospho-activation of MITOGEN-ACTIVATED PROTEIN KINASEs (MAPKs) is required for WAK2-mediated signaling in plants upon dmPectin sensing (Kohorn et al., 2009). We tested if RFO1 is similarly responsible for MAPK activation upon dmPectin sensing. MAPK6 and MAPK3 increased their phosphorylation status in WT roots after 30 min of exogenous dmPectin treatment, suggesting that dmPectin signal regulate MAPK cascades (Fig. 4A and B), as previously suggested for MAPK3 (Kohorn et al., 2009). In contrast, *rfo1-1* roots showed increased basal MAPK phosphorylation that did not undergo the same degree of activation after treatment with dmPectin (Fig. 4A and B). These results suggest that loss of RFO1 triggers increased basal MAPK phosphorylation and prevents its upregulation in response to dmPectin.

MAPK signal pathways activation is involved in the regulation of gene expression upon abiotic and biotic stress, including pectin oligomers (Aziz et al., 2004; Devendrakumar et al., 2018; Fan et al., 2017; Nakagami et al., 2005; Ren et al., 2008)**.** To further characterize the RFO1-mediated signaling cascade in Arabidopsis response to dmPectin, we quantified the expression of genes involved in pectin sensing and defense against Fo. These include the pectin receptors *WAK2* and *RLP44*, the defense-related transcriptional regulators *WRKY45* and *WRKY53*, and the phytohormone regulatory/biosynthesis genes *JASMONATE-ZIM-DOMAIN 10 (JAZ10)*, *DWARF 4 (DWF4)*, and *PHYTOALEXIN DEFICIENT 4 (PAD4)* (Choe et al., 1998; Kohorn et al., 2009; Lyons et al., 2015; Menna et al., 2021; Wolf et al., 2014; Zhou et al., 1998)**.** Exogenous treatment with dmPectin induced the expression of the receptors *WAK2* and *RLP44*, and the jasmonic acid and the salicylic acid response genes, *JAZ10* and *PAD4* respectively, in WT but not in *rfo1-1* roots (Fig. 4C). In contrast, *RFO1* expression did not change upon treatment with dmPectin (Fig. 4C). Altogether, our data indicate that RFO1 might regulate the gene expression of specific genes (*WAK2*, *RLP44*, *JAZ10*, and *PAD4*) in response to changes of pectin methylation through the regulation of MAPK3 and MAPK6 phosphorylation status. In addition, the misregulation of the defense related genes *WAK2, JAZ10, and PAD4* in the absence of RFO1 could contribute to the susceptibility phenotypes observed in *rfo1-1*.

RFO1 lifetime at the PM is altered by dmPectin fluxes

Signal perception can modify the nanoscale organization of receptors at the PM, influencing the corresponding downstream signaling (Gronnier et al., 2022; Jaillais and Ott, 2020; Pan et al., 2020). Thus, we tested whether the RFO1 dwell time and dynamics at the PM is altered by sensing dmPectin (Movie S1). To do that, a previously characterized estradiol-inducible construct overexpressing *PMEI5* (iPMEIox; Wolf et al., 2012) was introduced into the RFO1-GFP plant background (*rfo1-1* RFO1-GFP iPMEIox). The presence of RFO1 in the PM was studied using time-lapse movies of RFO1-GFP during three minutes (Movie S2), from which kymographs were obtained to quantify the dwell time of the corresponding foci. These kymographs analysis revealed an increase in the dwell time of the RFO1 particles at the PM when *PMEI5* was overexpressed (7.42 ± 0.24 s and 8.73 ± 0.49 s in control and iPMEIox background, respectively) that was reversed by dmPectin co-treatment (7.12 ± 0.34 s) (Fig. 5A and B). Single-particle tracking confirmed the kymograph observations (Fig. 5B and C) and showed that, although the number of RFO1-GFP particles at the PM did not differ between conditions, *PMEI5* overexpression increased the number of middle- (>50 s) and long-lived (>100 s) RFO1 particles (Fig. 5D). Co-treatment with dmPectin also reversed the effect of

iPMEIox (Fig. 5B-D), suggesting that a rise of mPectin levels increases the dwell time of RFO1-GFP at the PM. On the other hand, the instantaneous diffusion coefficients of RFO1-GFP particles were not significantly different between genotypes or treatments (Fig. 5E). These data indicate that *in vivo* RFO1-GFP particle dwell time but not lateral diffusion at the PM is dependent on the pectin methylation status.

RFO1 and RLP44 are required for plant response to genetic changes in pectin methylation at the CW, but only RFO1 participates in defense against Fo

Our data indicate that RFO1 is required for plant response to PME-induced pectin perturbation (Fig. 2), similar to the previously described PM-localized receptors RLP44 and BRI1 (Wolf et al., 2014)**.** Thus, to test the potential role of RFO1 in BR signaling to maintain CW integrity, we investigated the gene expression of BR signaling related genes such as *BR6ox2*, *CPD*, *CYP90D1*, *DWF4* and *PME3* (Wolf et al., 2012) in WT, PMEIox and *rfo1-1* PMEIox seedlings. The overexpression of *PMEI5* reduced significantly the expression of *BR6ox2*, *CPD* and *PME3*, and partially attenuated the expression of CYP90D1 and DWF4 (Fig. S5A), confirming previous results (Wolf et al., 2014) in the *rfo1-1* mutant background (Fig. S5A). These data suggest that RFO1, like RLP44, is also necessary to regulate the BR signaling in response to inhibition of pectin de-methylesterification in the CW.

Consequently, we evaluated if the common role of RFO1 and RLP44 extends beyond BR-mediated pectin signaling and into defense against Fo. The null RLP44 mutant, *rlp44-3 (Wolf et al., 2014)***,** showed no changes in susceptibility to Fo5176 vascular colonization at 7dpt but was more resistant than WT at earlier time points (Fig. S5B). These results indicate that, despite the similar roles that RFO1 and RLP44 seem to play in pectin integrity sensing within the context of PMEIox*,* they appear to have opposite functions in plant defense to Fo. Additionally, we tested the susceptibility to Fo5176 of the hypomorphic BRI1 mutant, *bri1-301* (Xu et al., 2008) and *bak1-5* mutant (Schwessinger et al., 2011). Plate infection assays demonstrated that *bri1-301* had increased resistance and *bak1-5* was more susceptible to Fo5176 vascular colonization (Fig. S5B), suggesting a positive role of BAK1 in defense against this fungus vs the activation of the receptor BRI1.

Discussion

The capacity of organisms to integrate external and internal cues for proper development in a constantly changing environment is essential for their survival, particularly for sessile ones, yet is far from being completely understood. A critical element for this phenotypic plasticity is the ability to respond to the changes in the CW properties caused by those cues. Effective sensing of plant cell wall integrity, becomes even more important during root colonization by vascular pathogens like Fo. These microbes extensively remodel the plant CWs and the host needs to balance defense and growth (Dora et al., 2022; Lionetti and Metraux, 2015; Vaahtera et al., 2019). Previous studies demonstrated that RLKs, WAKs, and WAKLs receptors are involved in detecting changes in the pectin at the CW during plant growth and defense responses, but the molecular mechanisms behind these functions have remained unresolved. Our data demonstrate that the PM-localized WAKL, RFO1, binds to dmPectin and this capacity of sensing the pectin methylation status is required for both plant development and resistance to root vascular fungi (Fig. 6).

Since its identification as an essential element of Arabidopsis resistance to Fo and Vd in 2005 (Diener and Ausubel, 2005; Verica and He, 2002), RFO1 has not been further characterized. Here we describe its molecular function at a high spatial and temporal resolution. Our work clarifies RFO1's role in root response to vascular fungi before the intruder reaches the xylem (Fig. 1A-C). Fo infection produces root growth inhibition similar to that observed after other microbe infections or cellular damage (MAMPs and DAMPs, respectively) (Gómez-Gómez et al., 1999; Huerta et al., 2020; Kesten et al., 2019; Poncini et al., 2017). The absence of RFO1 displayed a delay in the root growth inhibition induced by Fo, as reported in MAMPs-receptor mutants exposed to their corresponding MAMPs. The PM localization of RFO1 (Fig. 1E-G and S1C-F) hints that its function is important to detect the pathogen after the first interaction and slow-down its growth towards the vasculature.

Inhibition of PME activity, by both PMEI overexpression or exposure to EGCG, and its consequent reduction of dmPectins levels, also impairs root development (Wolf et al., 2012). These phenotypes were not observed in the *rfo1-1* mutant (Fig. 2), indicating that RFO1 is crucial to detect changes in pectin methylation in the CW. Root vascular fungi also alter the CW pectin methylation state during plant colonization (Fan et al., 2017), generating putative signals perceived by RFO1 through its extracellular domain ($RFO1^{ECD}$). Indeed, the Arabidopsis ecotype analysis presented here and based on previous studies of natural variation in plant defense to Fo (Diener and Ausubel, 2005) indicate that RFO1 might be involved in plant defense to Fo by recoginizing Fo-induced alterations to the pectin methylation status through its ECD. The same $RFO1^{ECD}$ is involved in plant response to genetic and chemical PME inhibition (Fig 3A-C and S2). Through *in vitro* experiments, we confirmed the capacity of $RFO1^{ECD}$ to bind dmPectin and showed that Fo infection altered the pectin methylation status at the CW (Fig. 3 and S4). Further research will be necessary to better understand the molecular basis behind $RFO1^{ECD}$ role in dmPectin sensing, by solving its structure and evaluating the function of its allelic diversity within Arabidopsis ecotypes. Furthermore, the ability of RFO1 to provide broad resistance to Fo and Verticillium sps. in Arabidopsis, reinforces the idea of RFO1 as pectin integrity rather than specific fungal factor recognizer (Li et al., 2020).

Our results confirm that WAKLs, like WAKs, can associate with pectin and share their preference for dmPectin over mPectin as a ligand (Fig 3E and F; Fig 6A; (Decreux and Messiaen, 2005; Kohorn et al., 2009)). RFO1-mediated perception of dmPectin promotes increased MAPK3 and MAPK6 phosphorylation and transcriptional changes (Fig. 4). Unlike RFO1, other members of the WAK family such as WAK2, mediate the perception of dmPectin only through MAPK3 activation but not MAPK6 (Kohorn et al., 2009), suggesting an expanded role of RFO1 in pectin sensing. In addition, RFO1 modulates the expression of *WAK2* and *RLP44* in response to altered pectin methylation status, suggesting a role for RFO1 upstream these receptors in pectin-integrity sensing. Moreover, the presence of RFO1 in the PM is dependent on the amount of dmPectin in the CW. The short-term and local reduction on dmPectin in PMEIox-induced seedlings increased the dwell time of RFO1 at the PM (Fig. 5), potentially altering RFO1's ability to interact with signaling partners to regulate downstream signaling cascades(Fig. 6B and C). A similar mechanism has been reported for other PM receptors such as BRI1 and PEPR1 (Gadeyne et al., 2014; Ma et al., 2020; Ortiz-Morea et al., 2016; Zhou et al., 2018). Considering the role of WAK2 and RLP44 in plant responses to alterations in pectin methylation, these receptors and RFO1 could work together in coordinating plant responses to alterations in pectin methylation at the CW (Kohorn et al.,

2009; Wolf et al., 2014). Additionally, as both RFO1 and RLP44 mediate PMEIox/EGCG phenotypes connecting with the BR signaling pathway (Wolf et al., 2014), RFO1 might be the upstream sensor of these perturbations that transmits the signal to the RLP44-BRI1-BAK1 complex (Fig. 6B). Another interesting possibility is that RFO1 and RLP44 could compete for dmPectin ligands at the plant CW upon constitutive PME inhibition. However, to address these different scenarios, further investigation is needed.

In regards to plant defense, RFO1 is required for transcriptional activation of the JA transcriptional suppressor, *JAZ10,* and the SA activation gene, *PAD4,* upon dmPectin treatment i(Fig. 4). Both pathways have been shown to be regulated through MAPK activation (Brodersen et al., 2006; Hettenhausen et al., 2015). Furthermore, the JA signaling pathway has recently been shown to participate in Arabidopsis root defense to Fo vascular penetration (Menna et al., 2021). Therefore, the activation of the JA and SA signaling pathways during RFO1-mediated dmPectin sensing could serve to boost defense responses against root vascular fungi, as suggested for other WAKs in cotton (Yang et al., 2021). Importantly, although *rfo1-1* response to PME inhibition mimics those reported for *rlp44* and *bri1-301* (Fig. 2; (Wolf et al., 2012, 2014)), this is not the case in defense to Fo, where *rlp44-3* and *bri1-301* are more resistant and *bak1-5* is more susceptible to the fungus than WT plants (Fig S5B). Therefore, we hypothesize that RFO1 participates in a BAK1-dependent Fo-defense signaling cascade at least partially different to that activated in response to PME inhibition (Fig 6C). One possibility is that, as suggested for other WAKs, RFO1 might contribute to plant response to an additional signal together with dmPectin, like OGs or MAMPs, to distinguish biotic stress from cell expansion cues (Kohorn et al., 2014; Qi et al., 2021; Wang et al., 2020).

Taken together, our work demonstrates for the first time that Fo-induced changes in pectin methylation at the PM are sensed by a receptor, which is required for plant defense. The RFO1 is a novel WAKL sensor of demethylated pectin, whose dwell time at the PM is altered by those pectin modifications, showing for the first time that a CW sensor dynamically responds to CW-derived signals. RFO1-dmPectin interaction initiates the activation of a MAPK-dependent signaling cascade and the upregulation of defense players and receptors involved in pectin perception. Additionally, RFO1 is a novel positive regulator of BR signaling required for normal growth upon alterations on PME activity and it also seems to be required for a BAK1-dependent defense to Fo infection. In conclusion, RFO1s dual functionality in development and defense seems to contribute to ensuring CW homeostasis during plant growth and response to biotic stress.

Author contributions

A.I.H. and C.S.R. conceived the study; A.I.H., C.S.R., J.C.M., and J.S. designed experiments; K.C. and R.S. provided essential material; A.I.H., J.C.M., G.S.A., J.S.N., and T.A. performed the experiments; A.I.H, J.C.M., G.S.A., and J.S.N. and analyzed the data; A.I.H., J.C.M., G.S.A., and C.S.R. wrote the manuscript with comments from J.S.N., K.C. and J.S.

Acknowledgments

We would like to thank Dr. Sebastian Wolf (University of Heidelberg, DE) for donating plant material used in this work, Dr. Alexandra Menna (ETH Zurich,CH) for the generation of plant glycoprotein extracts, Dr. Julien Gronier (UZH, CH) for his advice regarding single-particle

tracking, and the ScopeM (ETH Zurich, CH) for their assistance and service in the microscopy of plant cells. We also are very grateful to the Plant Cell Biology laboratory at ETHZ, Dr. Sebastian Wolf, Prof. Olivier Voinnet (ETH Zurich, CH), and prof. Cyril Zipfel (UZH, CH) for fruitful scientific discussion. **Funding:** The work described in this paper was supported by the Swiss National foundation and the Heinz Imhof Foundation to CSR. (2-72160-16 to AIH, SNF 31003A_163065/1 and SNF 310030_184769 to GS), the Peter und Traudl Engelhorn-Stiftung to CK, and the the European Research Council (ERC) grant agreement no. 716358 and the Fondation Philanthropique Famille Sandoz to J.S.

Declaration of Interests

The authors declare no competing interests.

MAIN FIGURE TITLES AND LEGENDS

Figure 1. The plasma membrane-localized RFO1 is required for plant resistance to Fo5176 pSIX1::GFP during root colonization.

(A) Representative images of 8-day old mock (-) or Fo5176 pSIX1::GFP infected (+) wild type (WT; Col-0), *rfo1-1*, and RFO1-GFP (*rfo1-1* pRFO1::RFO1-GFP) seedlings after 3 days post-transfer (dpt) to the corresponding treatment. Scale bar = 10 mm. **(B)** Root growth of Fo5176-infected seedlings relative to mock-treated ones, as shown in (A), between 0-3 dpt and 3-7 dpt. Data represent the mean ±SE of N > 40 seedlings per genotype from N = 3 independent replicates. RM ANOVA with Dunnett's multiple comparison test, p-value ** < 0.01. Significance shown compared to WT. **(C)** Cumulative Fo5176 vascular penetrations per root in plants infected as depicted in (A) from 3 to 7 dpt. Data represent the mean ±SE of N > 40 seedlings per genotype from N = 3 independent replicates. RM ANOVA with Dunnett's multiple comparison test, p-values **< 0.01, ***<0.001, ****<0.0001. ns, no significance. Significance shown compared to WT. **(D)** *RFO1* expression relative to *GADPH* in mock and Fo5176-infected WT roots at 2 and 3 dpt, as shown in (A). Bars represent the mean ±SE of N = 3 independent replicates, normalized to mock values. Pairwise *t*-test, p-values *< 0.05, **<0.01. **(E)** Representative longitudinal optical cross-section (top) of an elongating epidermal cell from a 5-day old RFO1-GFP root (green) after staining with FM4-64 (magenta), with the corresponding GFP and RFP gray value plot (bottom) taken along the labeled dashed yellow line. The arrows represent the margins of the plasma membrane. Scale bar = 10 µm. **(F)** Representative spinning disc confocal image and kymograph along the length of the dashed yellow line of a 5-day old RFO1-GFP root elongating epidermal cell from the corresponding movie (n = 50 frames, t = 50 s), showing RFO1 localization at discrete plasma membrane foci. Scale bar = 5 µm. **(G)** Dwell time frequencies of RFO1-GFP foci at the plasma membrane (PM) as depicted in (F). Mean (µ) is shown by a dashed blue line centered at 4.89 s. Data is derived from N > 4000 particles from 10 cells across 3 roots.

Figure 2. *rfo1-1* mutation alters plant response to perturbation of pectin methylation at the cell wall.
(A) Representative image of 8-day old wild type (WT; Col-0), *rfo1-1*, and RFO1-GFP (*rfo1-1* pRFO1::RFO1-GFP) seedlings after a 48h mock (-) or 6.25 µM EGCG (+) treatment. Scale bar = 5 mm. **(B)** Root growth of seedlings exposed to EGCG relative to mock-treated ones as depicted in (A). Data represent the mean ±SE of N ≥ 38 seedlings per genotype from 4 independent replicates. One-way ANOVA with Dunnett's multiple comparison test, p value ****<0.0001. Significance shown compared to WT. **(C)** and **(D)** Representative images of WT, PMEIox, *rfo1-1*, *rfo1-1* PMEIox and *rfo1-1* RFO1-GFP PMEIox of 8-day old seedlings (C) or 8-week old plants (D). In (C), scale bar = 5 mm.

Figure 3. The Col-0 extracellular domain of RFO1 binds to commercial and Arabidopsis cell wall-derived dmPectin
(A) Cumulative vascular penetrations observed in wild type (WT; Col-0), *rfo1-1*, RFO1^{Col-0}-GFP (*rfo1-1* RFO1^{Col-0}-GFP), and RFO1^{eckt}-GFP (*rfo1-1* RFO1^{eckt}-GFP) roots between 3 and 7 dpt to plates containing Fo5176 pSIX1::GFP microconidia. Data represent the mean ± SE of N ≥ 10 seedlings per genotype from 3 independent replicates. RM ANOVA with Tukey's multi-comparison post-hoc test, p-values **< 0.01, ***<0.001. Significance shown compared to WT. **(B)** Representative images of 8-day old WT, PMEIox, *rfo1-1*, *rfo1-1* PMEIox, *rfo1-1* RFO1^{Col-0}-GFP PMEIox, and *rfo1-1* RFO1^{eckt}-GFP PMEIox seedlings. Scale bar = 5 mm. **(C)** Relative root growth of EGCG-treated WT, *rfo1-1*, RFO1^{Col-0}-GFP, and RFO1^{eckt}-GFP roots as a percent of mock. Bars represent the mean ± SE of >15 seedlings per genotype from four biological replicates. One-way ANOVA with Dunnett's multiple-comparison post-hoc test, p-values, ****<0.0001. Significance indicated is compared to WT. **(D)** Representative dot immunobinding assay of immobilized commercial demethylesterified pectin (dmPectin) and methylated pectin (mPectin) probed with RFO1^{ECD}-SNAP or SNAP recombinant proteins. Protein binding was detected using a αSNAP antibody. **(E)** Quantification of dot immunobinding assay intensities in mean gray values from blots as shown in (D). **(F)** Representative dot immunobinding assay of immobilized plant CW fractions from mock and Fo5176-infected WT roots at 4dpt and probed with JIM5 or JIM7 antibodies. **(G)** Quantification of dot immunobinding assays intensities as a percent of mean gray values from blots as depicted in (F). **(H)** Representative dot immunobinding assay using root CW fractions as described in (F) and Fo5176 hyphae CW fractions probed with RFO1^{ECD}-SNAP recombinant protein. Protein binding was detected using a αSNAP antibody. **(I)** Quantification of dot immunobinding assays intensities as a percent of mean gray values from blots as shown in (E). (E, G, and I) Box plots: centerlines show the medians; means marked by +; box limits indicate the 25th and 75th percentiles; whiskers extend to the minimum and maximum. N ≥ 12 from ≥ 3 replicates independent replicates, 2-way ANOVA with Tukey's multiple comparison test, p-values *< 0.05, ***<0.001, ****<0.0001.

Figure 4. *rfo1-1* has altered basal and dmPectin-induced MAPK phosphorylation levels and gene expression activation

(A) Representative MAPK activation assay showing phospho-activated (Active) and Total levels of MAPK6, MAPK3, and MAPK4 in 8-day old roots of wild type (WT; Col-0) and *rfo1-1* plants treated with mock (-) or 10 µg/ml of dmPectin (+) for 30 min. **(B)** Quantification of relative MAPK activation in blots as shown in (A). Within each blot, relative MAPK activation was determined by referring Active to Total MAPK intensities per sample and these Active/Total data were normalized to the untreated WT. Data represent the mean ±SE of N=5 independent replicates. Multiple-comparison *t*-tests were performed within WT or *rfo1-1* samples in respect to their mock (black) or within WT and *rfo1-1* samples (blue), p-values *< 0.05, ***<0.001. **(C)** *WAK2, RLP44, WRKY45, WRKY53, JAZ10, DWF4, PAD4* and *RFO1* gene expression relative to *GAPDH* in 8-day old roots of WT and *rfo1-1* plants mock or dmPectin treated. The expression values were then normalized to mock WT. Data represent the mean ±SE of N = 3 independent replicates. Two-way ANOVA with Dunnett's multiple comparison test against WT mock per gene, p-values *< 0.05, **<0.01.

Figure 5. RFO1-GFP particle dwell time at the plasma membrane is altered by the perturbation of cell wall pectin methylation.

(A) Representative spinning disc confocal images (top) and kymographs (bottom) along the length of the dashed yellow lines of a 5-day old root elongating epidermal cells from the corresponding movie (n = 50 frames, 1 frame/s) of RFO1-GFP (*rfo1-1* pRFO1::RFO1-GFP) and RFO1-GFP iPMEIox (*rfo1-1* pRFO1::RFO1-GFP iPMEIox) seedlings treated with 12 µM estradiol for 2h. RFO1-GFP iPMEIox seedlings were co-treated with mock (-) or 10 µg/ml of dmPectin (+). Unless specified, all data derived from 180 s movies taken at 1 frame/s. Scale bar = 5 µm. **(B)** Dwell time frequencies of RFO1-GFP particles at the plasma membrane (PM) as depicted in (A). Means (µ) are shown by dashed lines. For each condition, data represents N >12000 particles from a minimum of 3 cells per root and 3 roots. **(C)** Average RFO1-GFP particle dwell times at the PM. **(D)** Quantification of RFO1-GFP total particles at the PM (left), and particles with dwell times >50 s (middle) and >100 s (right). **(E)** Average instantaneous diffusion coefficients of RFO1-GFP particles at the PM. **(C to E)** Data represent the mean ±SE of N >25 cells per condition from three independent replicates using 3 cells per root, 3 roots per condition, and tracking ≥ 1072 particles/cell, obtained from movies as described in (A). One-way ANOVA with Dunnett's multiple comparison test, p-values **<0.01, ****<0.0001.

Figure 6: Model of RFO1 signaling at the plasma membrane

A. Pectin is secreted to the CW heavily methyl- and acetyl-esterified. RFO1 binds dmPectin in the CW and acts as a sensor of the methyl-esterification level of pectins. **B.** When amounts of dmPectin decrease at the CW, as observed in plants overexpressing PMEI (PMEIox) or during EGCG treatment, RFO1 increases its dwell time at the plasma membrane, and triggers BR signaling, which is translated in a reduction of plant growth. RFO1 might be part of the RLP44-BRI1-BAK1 complex in this signaling process (dashed double arrow) **C.** In the presence of high levels of dmPectin, as observed during Fo infection or exogenous dmPectin treatment, RFO1 might release signaling partner(s) like WAK2 (dashed) to increase MAPK activation and downstream gene expression of defense-related genes. In the absence of RFO1, those potential signaling partners (i.e. WAK2) are constitutively free of RFO1-mediated repression leading to increased basal levels of MAPK phosphorylation. RFO1 detection of dmPectin is required to upregulate that MAPK signaling cascade and activate defense responses. RFO1-sensing of Fo might induce direct or indirect association with BAK1 (dashed

double arrow) and its dissociation from the RLP44-BRI1 complex, leading to defense response and growth inhibition.

STAR* METHODS

Plant material and growth

Arabidopsis thaliana plants used in these experiments, all Col-0 ecotype unless indicated (Ty-0), were grown at 16-h light (24° C)/8-h dark (21º C) cycle. *In vitro* experiments were carried out in ½ MS media plates (pH 5.7, not buffered; Duchefa #M0222.0025) supplemented with 1% (w/v) sucrose (when indicated) and 0.9% bacteriological grade agar (Difco #214530). *rfo1-1* (SALK_077975; (Diener and Ausubel, 2005), *PMEIox* (Wolf et al., 2012), *rlp44-3* (Wolf et al., 2014), *bri1-301 (Xu et al., 2008),* and *bak1-5 (Schwessinger et al., 2011)* lines were previously described. *rfo1-1* pRFO1::RFO1-GFP, *rfo1-1* pRFO1::RFO1$^{Ty\text{-}0}$-GFP*, rfo1-1* pRFO1::RFO1^{eckt}-GFP and pRFO1:RFP-N7 plants (see below under "Generation of constructs") were obtained by transformation according to standard procedures (Hellens et al., 2000). Transgenic lines were selected on soil based on resistance to 0.2% BASTA. Resulting heterozygous seedlings were screened for GFP or RFP fluorescence before continuing to select homozygous lines through BASTA selection and genotyping.

Fungal strains,culture conditions and plate infection assays.

Fo f.sp. *conglutinans* (Fo5176) pSIX1::GFP (Kesten et al., 2019) was used in this study. Fungal strains were cultured, microconidia were obtained and plate infection assays were performed as previously described (Huerta et al., 2020).

Generation of constructs

The *pRFO1::RFO1-GFP* construct was generated and assembled using Gateway cloning. To obtain the *pRFO1-GFP* destination vector, a 833 bp promoter region upstream of the *RFO1* (AT1G79670) ORF was amplified from Col-0 gDNA using primers 1 and 2 (Table S2) and ligated (NEBuilder® #E5520S) into the Gateway pUBC-GFP plasmid (Grefen et al., 2010) after removal of the original *UBQ* promoter by digestion (SacI+XhoI). The RFO1 ORF was amplified from Col-0 gDNA using primers 3 and 4 (Table S2) and cloned into the *pENTR/TOPO-D/SD* Gateway vector according to the std. TOPO PCR cloning protocol. A Gateway LB reaction was performed using the resulting *pRFO1-GFP* destination and p*ENTR-RFO1* plasmids and transformed into DH5α *Escherichia coli* cells. *pRFO1::RFO1-GFP E. coli* transformants were selected through spectinomycin selection.

pRFO1::RFO1$^{Ty\text{-}0}$-GFP and *pRFO1::RFO1^{eckt}-GFP* constructs were generated using the same method described above. The *RFO1$^{Ty\text{-}0}$* ORF was amplified from Arabidopsis Ty-0 ecotype cDNA using primers 5 and 4 (Table S2). The *RFO1^{eckt}* chimera was generated by amplifying the Col-0 RFO1 ectodomain and transmembrane domains using primers 3 and 7, and the Ty-0 cytosolic domain using primers 6 and 4. The resulting two fragments were then ligated through an elongation PCR employing primers 3 and 4. A Gateway LB reaction was performed using the *pRFO1-GFP* destination vector and the resulting *pENTR-RFO1^{Ty}-0* and *pENTR-RFO1^{eckt}* plasmids were transformed into DH5α *E. coli* cells. Transformants were selected through spectinomycin selection.

A new vector that we named "pNew"was generated by digesting pGreenII with NotI and EcoRI. A new insertion was designed and ordered as a gene fragment containing the Arabidopsis

thaliana ubiquitin-10 promoter (Grefen et al., 2010) followed by a multiple cloning site and the Arabidopsis thaliana HSP-terminator (Nagaya et al., 2010) for convenient insertion of genes under control of the ubiquitin-10 or native promoter by cutting the vector with either BamHI and XbaI or EcoRI and XbaI, respectively. The *pRFO1::RFP-N7* construct was generated using primers 8-13 (Table S2) by amplifying the *RFO1* promoter as described above, the *RFP from* pUBN-RFP-Dest (Grefen et al., 2010), and the *N7* nuclear targeting sequence from AT4G19150, respectively. The fragments were cloned into a predigested pNew (EcoR1 and Xba1) and ligated in a one-step ligation (NEBuilder® #E5520S). The resulting construct was then transformed into DH5α E. *coli* cells and selected for resistance to kanamycin.
All the above constructs were transformed into electrocompetent GV31 *Agrobacterium tumefaciens* (together with pSOUP for *pRFO1::RFP-N7*) and selected using their respective antibiotic plus 25 ug/ml gentamicin and rifampicin.

Recombinant protein production and purification

Codon-optimized synthetic genes for expression in *Spodoptera frugiperda* (Invitrogen GeneArt), coding for the ectodomain of RFO1 (residues 28 to 347; AT1G79670) with a SNAP-tag C-terminal fusion was cloned into a modified pFastBac (Geneva Biotech) vector providing a TEV (tobacco etch virus protease) cleavable C-terminal StrepII-9xHis tag. For protein expression, *Trichoplusia ni* Tnao38 cells were infected with the RFO1-SNAP virus and incubated for one day at 28 ºC and 2 extra days at 22 ºC at 110 rpm. The secreted RFO1-SNAP (under the 30K signal peptide) was purified from the supernatant by sequential Ni^{2+}(HisTrap excel; GE Healthcare; equilibrated in 25 mM KPi pH 7.8, 500 mM NaCl) and StrepII (Strep-Tactin Superflow high capacity [IBA Lifesciences] equilibrated in 25 mM Tris pH 8.0, 250 mM NaCl, 1 mM EDTA) affinity chromatography. SNAP-tag was cloned into a modified pETM11 vector, providing a C-terminal TEV site and StrepII-9xHis tag. The SNAP protein was purified from *E. coli* cells following the same procedure described above. Both proteins were incubated with TEV protease to remove the tags. Proteins were further purified by Size Exclusion Chromatography on a Superdex 200 increase 10/300 GL column (GE Healthcare), equilibrated in 20 mM HEPES pH 7.5, 150 mM NaCl (Fig. S3A and B). For biochemical experiments and quality control, proteins were concentrated using Amicon Ultra concentrators (Millipore, molecular weight cut-off 10,000and 30,000 Da). Also, proteins were analyzed for purity and structural integrity by sodium dodecyl sulfate (SDS)-polyacrylamide gel electrophoresis (Fig. S3A and B).

Generation of dmPectin and mPectin, CWl pectin fractions, and CW glycoprotein extracts

To produce dmPectin and mPectin samples, 1 mg/ml Apple-derived pectin (Sigma #93854) was dissolved in 50 mM NaOH or distilled water, respectively, and placed on ice for 60 min. Then, samples were dialyzed overnight at 4°C against distilled water in Spectra/Por® 3 pre-wet dialysis tubing (Spectrum #132720). Afterwards, they were transferred to a 50 ml conical tube, flash frozen, and lyophilized overnight. The lyophilized dmPectin and mPectin samples were then resuspended in 1 ml of 1.5 mM EDTA solution in water and stored at -20°C until use.

To produce CW fractions, CW alcohol insoluble residue (AIR) was first obtained as previously described (Menna et al., 2020) from mock and Fo5176-infected Arabidopsis roots at 4 dpt. Fractionation of 10 mg AIR proceeded as previously described (Hotchkiss and Hicks, 1990; Mort et al., 1991) (Fig S3B) with the following modifications. Fraction I was obtained by treating

the AIR with 1 ml of a 50 mM imidazole and 20 mM $NaBH_4$ solution at pH 7 at 4°C with rotation for 8 hrs. After centrifugation, the supernatant was transferred to a fresh tube, the pellet was treated once more as described above, and the supernatants combined and used as fraction I. The remaining pellet was used to obatined fraction II as done for fraction I, but using 50 mM Na_2CO_3 and 20 mM $NaBH_4$ solution instead of imidazole. The result pellet after two rounds of fraction II extraction was incubated with 1 M KOH and 20 mM $NaBH_4$ to obtained fraction III, following the same steps described for the previous fractions. The three fractions were neutralized using glacial acetic acid before transferring them to Spectra/Por® 3 pre-wet dialysis tubing for overnight dialysis at 4°C against distilled water. After dialysis, samples were transferred to a pre-weighed 50 ml conical tube, flash frozen, and lyophilized overnight. The lyophilized cell wall fractions were then weighed and resuspended with distilled water to a concentration of 1mg/ml and stored at -20°C until further use.

For CW glycoprotein (GP) extracts, leaves of 6-week-old WT plants were harvested and processed as previously described (Menna et al., 2021). The final lyophilized CW glycoproteins were weighed, flash frozen in liquid nitrogen, and stored at -80°C until use.

Dot immunobinding assays

For analysis of RFO1-SNAP and SNAP recombinant proteins interaction with pectins and plant CW-derived samples, 15 µg of plant CW material (fractions or GP extracts) per sample were immobilized in triplicates onto nitrocellulose membranes using a Hybri-dot manifold (BRL #1050MM) under light vacuum and air-dried at room temperature for 30 minutes. The dot blot membranes were blocked with 5% bovine serum albumin (Sigma #A9647) for 1 h, quickly washed in a sodium acetate buffer (NaAc 20mM; pH 5.4), and incubated overnight at 4°C with fresh 300 µM solutions of RFO1-SNAP or SNAP in NaAc buffer. The blots were washed three times with NaAc buffer and incubated with αSNAP antibody (NEB P9310S) at a 1:5000 dilution in TBST (25mM Tris-HCl pH 7.5, 100mM NaCl, 0.05% Tween20) for 1 h. After washing, the membranes were probed with Rabbit-HRP antibody (Azure #AC2114) at a 1:10000 dilution in TBST for 1 h, washed in TBST for 4 h, and developed with 1 ml of the HRP substrate. Chemiluminescence was detected for 500 s using a Bio-Rad ChemiDoc™Touch imaging system. Dot blot images were analyzed using Fiji according to the protocol Dot Blot Analysis (nih.gov) with the following modifications. Background subtraction was performed using a 20-pixel radius rolling ball. Data derived from Arabidopsis CW components, the average gray value of each sample is shown as a percentage of the total average signal of the corresponding fraction. For data derived from pure pectin samples, the average gray values were shown unnormalized.

For blots using JIM5 and JIM7 antibodies, 15 µg of carbohydrate material per sample were immobilized in triplicates onto nitrocellulose membranes, blocked, and washed as indicated above. The dot blot membranes were incubated for 1 h with JIM5 (Megazyme AB-JIM5) or JIM7 (Megazyme AB-JIM7) antibodies at a 1:100 dilution in TBST, washed three times in TBST, and probed with Rat-HRP antibody (Azure AC2118) at a 1:10000 dilution in TBST for 1 h. The blots were washed in TBST for 1 hour before being exposed to the HRP substrate and analyzed following the aforementioned protocol.

Epigallocatechin gallate (EGCG) root growth inhibition assays

Two 5-day old seedlings grown on 1/2 MS agar + 1% sucrose plates were scanned and transferred to 12-well plates containing 2 mL of 1/2 MS +1% sucrose with or without 6.25 µM

EGCG (Sigma #E4143) and grown for 48 h under continuous light at 21°C with shaking at 70 RPM. Root length at the start of the experiment and after 48h of treatment was measured using the SNT plugin of Fiji application. Root growth inhibition of EGCG treated seedlings was calculated by dividing the average root length increase of every pair of roots treated with EGCG by the average root length increase of every pair of mock roots of its corresponding genotype.

Assessment of MAPK activation in response to dmPectin

Three to four 8-day old seedlings were transferred from agar plates to 6-well plates containing 2 ml of 1/2 MS, left to equilibrate at room temperature for 1 h, and treated for 30 min with 20 µl 1.5 mM EDTA with or without 1mg/ml dmPectin dissolved on it. 3 to 4 roots per genotype and condition were ground with Laemmli sample buffer plus silica sand using a mortar and pestle. The resulting extract was transferred to a centrifuge tube and boiled at 80°C for 5 min, centrifuged and 20 µl of each supernatant were subjected to SDS-PAGE on a 10% polyacrylamide gel. Proteins were transferred to nitrocellulose membranes using the Bio-Rad Trans-Blot® Turbo™ transfer system and protocol during 10 min transfer at 2.5V, blocked for 1 h using 5% milk protein in TBST, quickly washed with TBST, and incubated with P-p44/42 MAPK antibody (Cell Signal #9101) at a 1:500 dilution in TBST for 1 h to determine activated MAPK levels. Then, the blots were washed with TBST, incubated with Rabbit-HRP antibody (Azure #AC2114) at a 1:10000 dilution in TBST for 1 h, washed in TBST for 1 h and treated with 1 ml of HRP substrate. Chemiluminescence was detected for 60 s using a Bio-Rad ChemiDoc™Touch imaging system. Dot blot images were analyzed in Fiji using the Gel Tools plug-in after background subtraction using a 20-pixel radius rolling ball. To quantify the total MAPK protein levels in these samples, blots were then stripped for 30 min using 0.2 M glycine pH 2.2, blocked with 5% milk protein, incubated with p44/42 MAPK antibody (Cell Signal #9102) and subjected to the same washing, treatment, and imaging as above. The relative MAPK activation of each sample was normalized to the total MAPK intensity values per condition per genotype and blot, and then compared to WT.

Gene expression analysis by qRT-PCR

For gene expression analysis in response to dmPectin, 3-4 roots per condition and genotype grown and treated as described above (see “Assessment of MAPK activation in response to dmPectin”) were collected. Total RNA was extracted using TRIzol reagent (Thermo #15596026) and 1 µg per sample were treated with DNAse.

For *RFO1* expression quantification, roots of 8-day old mock and Fo5176-infected WT seedlings were harvested at 1-7 dpt. For gene expression analysis of PME3 and BR related genes, 100 mg root tissue was harvested. Total RNA was extracted using RNeasy Plant Mini Kit (Qiagen #74904) and treated with RNase-Free DNase Set (Qiagen #79254).

The first-strand cDNAs synthesized using the Maxima H Master Mix (Thermo #M1681) were amplified by RT-qPCR using SYBR green master mix (AB #4309155) in a 10 µl reaction using the primers indicated in Table S2: *RFO1* (primers 37-38), *WAK2* (primers 41-42 (Wolf et al., 2014)), *RLP44* (primers 39-40 (Wolf et al., 2014)), *WRKY45* (primers 43-44; (Souza et al., 2017)), *WRKY53* (primers 45-46 (Masachis et al., 2016)), *JAZ10* (primers 31-32 (Liu et al., 2016)), *DWF4* (primers 27-28 (Wolf et al., 2014)), *PAD4* (primers 35-36 (Chen et al., 2015)), *BR6ox2* (primers 21-22 (Shimada et al., 2003)), *CPD* (primers 23-24 (Shimada et al., 2003)), *CYP90D1* (primers 25-26 (Shimada et al., 2003)), *PME3* (primers 35-36 (Bethke et al., 2014)) and the reference gene *GAPDH* (primers 29-30; (Czechowski et al., 2005)) using a LightCycler 480 II (Roche). No-template controls and melting curves were examined to ensure no

contamination and primer–dimer formation was present. The 2ΔCT method was used to quantify the relative expression of each gene (Schmittgen and Livak, 2008).

Spinning disk live-cell imaging and single-particle tracking analysis

Roots of 5- day- old seedlings were covered with a 1% agarose cushion as described previously (Gutierrez et al., 2009). *rfo1-1* RFO1-GFP and *rfo1-1* RFO1-GFP iPMEIox seedlings were transferred to 6-well plates containing 2 ml of half MS with12 µM β-estradiol (Sigma #E8875; in DMSO) and 20 µl of 1.5 mM EDTA with or without 1 mg/ml dmPectin dissolved on it, and incubated for 2 h before imaging. RFO1-GFP particles were imaged with a CSU- W1 Yokogawa spinning disk head fitted to a Nikon Eclipse Ti- E- inverted microscope with a CFI PlanApo × 100 N.A. 1.40 oil immersion objective, two iXon Ultra EM- CCD cameras (Andor, GB), and a ×1.2 lens between the spinning disk and camera was used. For this system, GFP was imaged using a 488 nm solid- state diode laser and a 525/50 nm emission filter; RFP was detected with a 561 nm solid- state diode laser and a 630/75 nm emission filter. Time-lapse images were processed and analyzed with Fiji (Schindelin et al., 2012). Before particle tracking, drifts were corrected by using the plugin StackReg (Thevenaz et al., 1998). Backgrounds were subtracted by the "Subtract Background" tool (rolling ball radius 40 pixels). The tool "walking average" was additionally applied averaging three frames. Single-particle tracking was performed using the Fiji application, Trackmate (Tinevez et al., 2017) using the LAP tracker with a particle radius of 0.4 µm and an initial threshold of 15. Auto filtering based on signal quality was performed for each image. Cells were imaged for 180 s at 1 frame/s, 800 ms exposure, and a gain of 250. The generated spot and track data from Trackmate were used for dwell time, mean squared displacement (MSD), and log diffusion coefficient (Log(D)) calculations. All data analyses were performed For dwell time analysis, the particles already present at the PM when the movie started and those that were still visible when the movie finished were not considered for the analysis. using R (version 4.0.3) with R Studio (version 1.1.463) and images were made with ggplot2. nly tracks starting 1 second after the start of imaging and ending 1 second before the end of the imaging were included in the dwell time analysis. Middle- (>50 s) and long-lived (>100 s.) tracks were counted separately and compared to total filtered tracks from the dwell time analysis above. MSD values were derived from the spot data of all spots in a given movie. MSD and Log(D) were calculated as previously described (Wagner et al., 2017), using the following formulas:

(1) MSD= 1/(N-n) ∑_(i=1)^(N-n)▒〖|x_(i+n)- x_i |^2 ,n=1,…,N-1〗

(2) MSD =4DnΔt

Confocal microscopy

Root epidermal cells expressing *pRFO1:RFP-N7* were imaged with a Zeiss 780 confocal laser scanning microscope equipped with a 20x 0.5 NA objective. RFP was visualized using 561 nm laser excitation and 592–754 nm spectral detection. Z-stack images were taken, and image tiling and stitching was performed with the ZEN software (Zeiss). The images were further processed and analyzed with Fiji.

Resource availability

Lead contact: Further information and requests for resources and reagents should be directed to and will be fulfilled by the lead contact, Clara Sánchez-Rodríguez (clara_sanchez@ethz.ch).

Materials availability: This study did not generate new unique reagents

Data and code availability: All data reported in this paper will be shared by the lead contact upon request. This paper does not report original code. Any additional information required to reanalyze the data reported in this paper is available from the lead contact upon request.

SUPPLEMENTAL MOVIES

Movie S1: Dynamic Localization of RFO1-GFP at the plasma membrane. Related to Figure 1F-G

The movie depicts the dynamic behavior of RFO1-GFP expressed in *rfo1-1* in *Arabidopsis* root epidermal cells acquired using Spinning disc confocal microscopy. Foci identified by Trackmate using the LAP tracker to be analyzed are indicated in the right panel. This movie corresponds to Figure 1F and G.

Movie S2: Dynamic Localization of RFO1-GFP at the plasma membrane when dmPectin levels at the cell wall are altered. Related with Figure 5.

The movie depicts the dynamic behavior of RFO1-GFP expressed in *rfo1-1* in *Arabidopsis* root epidermal cells acquired using Spinning disc confocal microscopy. The pectin methylation level at the cell wall was modulated by introducing the line iPMEIox which was activated using estradiol (Mock; middle panel) to reduce the dmPectin levels. This effect was compensated by adding dmPectin (right panel). The control line is shown in the left panel. Scale bar = 5 um. This movie corresponds to Figure 5.

REFERENCES

Albersheim, P., Darvill, A.G., O'Neill, M.A., Schols, H.A., and Voragen, A.G.J. (1996). An hypothesis: The same six polysaccharides are components of the primary cell walls of all higher plants. In Progress in Biotechnology, J. Visser, and A.G.J. Voragen, eds. (Elsevier), pp. 47–55.

Anderson, C.T. (2016). We be jammin': an update on pectin biosynthesis, trafficking and dynamics. J. Exp. Bot. *67*, 495–502.

Anderson, C.M., Wagner, T.A., Perret, M., He, Z.H., He, D., and Kohorn, B.D. (2001). WAKs: cell wall-associated kinases linking the cytoplasm to the extracellular matrix. Plant Mol. Biol. *47*, 197–206.

Aziz, A., Heyraud, A., and Lambert, B. (2004). Oligogalacturonide signal transduction, induction of defense-related responses and protection of grapevine against Botrytis cinerea. Planta *218*, 767–774.

Bethke, G., Grundman, R.E., Sreekanta, S., Truman, W., Katagiri, F., and Glazebrook, J. (2014). Arabidopsis PECTIN METHYLESTERASEs contribute to immunity against Pseudomonas syringae. Plant Physiol. *164*, 1093–1107.

Bidhendi, A.J., and Geitmann, A. (2016). Relating the mechanics of the primary plant cell wall to morphogenesis. J. Exp. Bot. *67*, 449–461.

Bishop, C.D., and Cooper, R.M. (1983). An ultrastructural study of root invasion in three vascular wilt diseases. Physiological Plant Pathology *22*, 15–IN13.

Bravo Ruiz, G., Di Pietro, A., and Roncero, M.I.G. (2016). Combined action of the major secreted exo- and endopolygalacturonases is required for full virulence of Fusarium oxysporum. Mol. Plant Pathol. *17*, 339–353.

Bravo-Ruiz, G., Sassi, A.H., Marcet-Houben, M., Di Pietro, A., Gargouri, A., Gabaldon, T., and Roncero, M.I.G. (2017). Regulatory Mechanisms of a Highly Pectinolytic Mutant of Penicillium occitanis and Functional Analysis of a Candidate Gene in the Plant Pathogen Fusarium oxysporum. Front. Microbiol. *8*, 1627.

Brodersen, P., Petersen, M., Bjørn Nielsen, H., Zhu, S., Newman, M.-A., Shokat, K.M., Rietz, S., Parker, J., and Mundy, J. (2006). Arabidopsis MAP kinase 4 regulates salicylic acid- and jasmonic acid/ethylene-dependent responses via EDS1 and PAD4. Plant J. *47*, 532–546.

Brutus, A., Sicilia, F., Macone, A., Cervone, F., and De Lorenzo, G. (2010). A domain swap approach reveals a role of the plant wall-associated kinase 1 (WAK1) as a receptor of oligogalacturonides. Proc. Natl. Acad. Sci. U. S. A. *107*, 9452–9457.

Casero, P.J., and Knox, J.P. (1995). The monoclonal antibody JIM5 indicates patterns of pectin deposition in relation to pit fields at the plasma-membrane-face of tomato pericarp cell walls. Protoplasma *188*, 133–137.

Chen, Q.-F., Xu, L., Tan, W.-J., Chen, L., Qi, H., Xie, L.-J., Chen, M.-X., Liu, B.-Y., Yu, L.-J., Yao, N., et al. (2015). Disruption of the Arabidopsis Defense Regulator Genes SAG101, EDS1, and PAD4 Confers Enhanced Freezing Tolerance. Mol. Plant *8*, 1536–1549.

Choe, S., Dilkes, B.P., Fujioka, S., and Takatsuto, S. (1998). The DWF4 Gene of Arabidopsis Encodes a Cytochrome P450 That Mediates Multiple 22α-Hydroxylation Steps in Brassinosteroid Biosynthesis. The Plant.

Cooper, R.M., and Wood, R.K.S. (1975). Regulation of synthesis of cell wall degrading enzymes by Veticillium albo-atrum and Fusarium oxysporum f. sp. lycopersici. Physiological Plant Pathology *5*, 135–156.

Czechowski, T., Stitt, M., Altmann, T., and Udvardi, M.K. (2005). Genome-wide identification and testing of superior reference genes for transcript normalization in Arabidopsis. Plant.

Decreux, A., and Messiaen, J. (2005). Wall-associated kinase WAK1 interacts with cell wall pectins in a calcium-induced conformation. Plant Cell Physiol. *46*, 268–278.

Decreux, A., Thomas, A., Spies, B., Brasseur, R., Van Cutsem, P., and Messiaen, J. (2006). In vitro characterization of the homogalacturonan-binding domain of the wall-associated kinase WAK1 using site-directed mutagenesis. Phytochemistry *67*, 1068–1079.

Devendrakumar, K.T., Li, X., and Zhang, Y. (2018). MAP kinase signalling: interplays between plant PAMP- and effector-triggered immunity. Cellular and Molecular Life Sciences *75*, 2981–2989.

Diener, A.C., and Ausubel, F.M. (2005). RESISTANCE TO FUSARIUM OXYSPORUM 1, a dominant Arabidopsis disease-resistance gene, is not race specific. Genetics *171*, 305–321.

Di Pietro, A., and Roncero, M.I. (1998). Cloning, expression, and role in pathogenicity of pg1 encoding the major extracellular endopolygalacturonase of the vascular wilt pathogen Fusarium oxysporum. Mol. Plant. Microbe. Interact. *11*, 91–98.

Dmochowska-Boguta, M., Kloc, Y., Zielezinski, A., Werecki, P., Nadolska-Orczyk, A., Karlowski, W.M., and Orczyk, W. (2020). TaWAK6 encoding wall-associated kinase is involved in wheat resistance to leaf rust similar to adult plant resistance. PLoS One *15*, e0227713.

Dora, S., Terrett, O.M., and Sánchez-Rodríguez, C. (2022). Plant-microbe interactions in the apoplast: Communication at the plant cell wall. Plant Cell.

Durrands, P.K., and Cooper, R.M. (1988). The role of pectinases in vascular wilt disease as determined by defined mutants of Verticillium albo-atrum. Physiol. Mol. Plant Pathol. *32*, 363–371.

Engelsdorf, T., Gigli-Bisceglia, N., Veerabagu, M., McKenna, J.F., Vaahtera, L., Augstein, F., Van der Does, D., Zipfel, C., and Hamann, T. (2018). The plant cell wall integrity maintenance and immune signaling systems cooperate to control stress responses in Arabidopsis thaliana. Sci. Signal. *11*.

Fan, H., Dong, H., Xu, C., Liu, J., Hu, B., Ye, J., Mai, G., and Li, H. (2017). Pectin methylesterases contribute the pathogenic differences between races 1 and 4 of Fusarium oxysporum f. sp. cubense. Sci. Rep. *7*, 13140.

Feng, W., Kita, D., Peaucelle, A., Cartwright, H.N., Doan, V., Duan, Q., Liu, M.-C., Maman, J., Steinhorst, L., Schmitz-Thom, I., et al. (2018). The FERONIA Receptor Kinase Maintains Cell-Wall Integrity during Salt Stress through Ca2+ Signaling. Curr. Biol. *28*, 666–675.e5.

Ferrari, S., Savatin, D.V., Sicilia, F., Gramegna, G., Cervone, F., and Lorenzo, G.D. (2013). Oligogalacturonides: plant damage-associated molecular patterns and regulators of growth and development. Front. Plant Sci. *4*, 49.

Gadeyne, A., Sánchez-Rodríguez, C., Vanneste, S., Di Rubbo, S., Zauber, H., Vanneste, K., Van Leene, J., De Winne, N., Eeckhout, D., Persiau, G., et al. (2014). The TPLATE adaptor complex drives clathrin-mediated endocytosis in plants. Cell *156*, 691–704.

Gámez-Arjona, F.M., Vitale, S., Voxeur, A., Dora, S., Müller, S., Sancho-Andrés, G., Montesinos, J.C., Di Pietro, A., and Sánchez-Rodríguez, C. (2021). Impairment of the cellulose degradation machinery enhances fungal virulence but limits reproductive fitness.

García-Maceira, F.I., Di Pietro, A., and Roncero, M.I.G. (2000). Cloning and disruption of pgx4 encoding an in planta expressed exopolygalacturonase from Fusarium oxysporum. Mol. Plant. Microbe. Interact. *13*, 359–365.

García-Maceira, F.I., and Di Pietro, A. (2001). Molecular Characterization of an Endopolygalacturonase from Fusarium oxysporum Expressed during Early Stages of Infection. Applied and.

Glass, N.L., Schmoll, M., Cate, J.H.D., and Coradetti, S. (2013). Plant cell wall deconstruction by ascomycete fungi. Annu. Rev. Microbiol. *67*, 477–498.

Glöckner, N., zur Oven-Krockhaus, S., Rohr, L., Wackenhut, F., Burmeister, M., Wanke, F., Holzwart, E., Meixner, A.J., Wolf, S., and Harter, K. (2020). Three-fluorophore FRET enables the analysis of ternary protein association in living plant cells.

Gómez-Gómez, L., Felix, G., and Boller, T. (1999). A single locus determines sensitivity to bacterial flagellin in Arabidopsis thaliana. Plant J. *18*, 277–284.

Gordon, T.R. (2017). Fusarium oxysporum and the Fusarium Wilt Syndrome. Annu. Rev. Phytopathol. *55*, 23–39.

Grefen, C., Donald, N., Hashimoto, K., Kudla, J., Schumacher, K., and Blatt, M.R. (2010). A ubiquitin-10 promoter-based vector set for fluorescent protein tagging facilitates temporal stability and native protein distribution in transient and stable expression studies. Plant J. *64*,

355–365.

Gronnier, J., Franck, C.M., Stegmann, M., DeFalco, T.A., Abarca, A., von Arx, M., Dünser, K., Lin, W., Yang, Z., Kleine-Vehn, J., et al. (2022). Regulation of immune receptor kinase plasma membrane nanoscale organization by a plant peptide hormone and its receptors. Elife *11*.

Gutierrez, R., Lindeboom, J.J., Paredez, A.R., Emons, A.M.C., and Ehrhardt, D.W. (2009). Arabidopsis cortical microtubules position cellulose synthase delivery to the plasma membrane and interact with cellulose synthase trafficking compartments. Nat. Cell Biol. *11*, 797–806.

He, Z.-H., Fujiki, M., and Kohorn, B.D. (1996). A Cell Wall-associated, Receptor-like Protein Kinase*. J. Biol. Chem. *271*, 19789–19793.

Hellens, R.P., Edwards, E.A., Leyland, N.R., Bean, S., and Mullineaux, P.M. (2000). pGreen: a versatile and flexible binary Ti vector for Agrobacterium-mediated plant transformation. Plant Mol. Biol. *42*, 819–832.

Hettenhausen, C., Schuman, M.C., and Wu, J. (2015). MAPK signaling: a key element in plant defense response to insects. Insect Sci. *22*, 157–164.

Hotchkiss, A.T., Jr, and Hicks, K.B. (1990). Analysis of oligogalacturonic acids with 50 or fewer residues by high-performance anion-exchange chromatography and pulsed amperometric detection. Anal. Biochem. *184*, 200–206.

Huerta, A.I., Kesten, C., Menna, A.L., Sancho-Andrés, G., and Sanchez-Rodriguez, C. (2020). In-Plate Quantitative Characterization of Arabidopsis thaliana Susceptibility to the Fungal Vascular Pathogen Fusarium oxysporum. Curr Protoc Plant Biol *5*, e20113.

Huertas-González, M.D., Ruiz-Roldán, M.C., García Maceira, F.I., Roncero, M.I., and Di Pietro, A. (1999). Cloning and characterization of pl1 encoding an in planta-secreted pectate lyase of Fusarium oxysporum. Curr. Genet. *35*, 36–40.

Jaillais, Y., and Ott, T. (2020). The Nanoscale Organization of the Plasma Membrane and Its Importance in Signaling: A Proteolipid Perspective. Plant Physiol. *182*, 1682–1696.

Jonkers, W., and Rep, M. (2009). Mutation of CRE1 in Fusarium oxysporum reverts the pathogenicity defects of the FRP1 deletion mutant. Mol. Microbiol. *74*, 1100–1113.

Kesten, C., Gámez-Arjona, F.M., Menna, A., Scholl, S., Dora, S., Huerta, A.I., Huang, H.-Y., Tintor, N., Kinoshita, T., Rep, M., et al. (2019). Pathogen-induced pH changes regulate the growth-defense balance in plants. EMBO J. *38*, e101822.

Klosterman, S.J., Atallah, Z.K., Vallad, G.E., and Subbarao, K.V. (2009). Diversity, pathogenicity, and management of verticillium species. Annu. Rev. Phytopathol. *47*, 39–62.

Knox, J.P., Linstead, P.J., King, J., Cooper, C., and Roberts, K. (1990). Pectin esterification is spatially regulated both within cell walls and between developing tissues of root apices. Planta *181*, 512–521.

Kohorn, B.D., Johansen, S., Shishido, A., Todorova, T., Martinez, R., Defeo, E., and Obregon, P. (2009). Pectin activation of MAP kinase and gene expression is WAK2 dependent. Plant J. *60*, 974–982.

Kohorn, B.D., Kohorn, S.L., Saba, N.J., and Martinez, V.M. (2014). Requirement for pectin methyl esterase and preference for fragmented over native pectins for wall-associated

kinase-activated, EDS1/PAD4-dependent stress response in Arabidopsis. J. Biol. Chem. *289*, 18978–18986.

Lally, D., Ingmire, P., Tong, H.Y., and He, Z.H. (2001). Antisense expression of a cell wall-associated protein kinase, WAK4, inhibits cell elongation and alters morphology. Plant Cell *13*, 1317–1331.

Li, J., Cornelissen, B., and Rep, M. (2020). Host-specificity factors in plant pathogenic fungi. Fungal Genet. Biol. *144*, 103447.

Li, L., Li, K., Ali, A., and Guo, Y. (2021). AtWAKL10, a Cell Wall Associated Receptor-Like Kinase, Negatively Regulates Leaf Senescence in Arabidopsis thaliana. Int. J. Mol. Sci. *22*.

Lin, W., Tang, W., Pan, X., Huang, A., Gao, X., Anderson, C.T., and Yang, Z. (2021). Arabidopsis pavement cell morphogenesis requires FERONIA binding to pectin for activation of ROP GTPase signaling. Curr. Biol.

Lionetti, V., and Metraux, J.-P. (2015). Plant cell wall in pathogenesis, parasitism and symbiosis (Frontiers Media SA).

Liu, L., Sonbol, F.-M., Huot, B., Gu, Y., Withers, J., Mwimba, M., Yao, J., He, S.Y., and Dong, X. (2016). Salicylic acid receptors activate jasmonic acid signalling through a non-canonical pathway to promote effector-triggered immunity. Nat. Commun. *7*, 13099.

Liu, N., Sun, Y., Pei, Y., Zhang, X., Wang, P., Li, X., Li, F., and Hou, Y. (2018). A Pectin Methylesterase Inhibitor Enhances Resistance to Verticillium Wilt. Plant Physiol. *176*, 2202–2220.

Lyons, R., Stiller, J., Powell, J., Rusu, A., Manners, J.M., and Kazan, K. (2015). Fusarium oxysporum triggers tissue-specific transcriptional reprogramming in Arabidopsis thaliana. PLoS One *10*, e0121902.

Ma, X., Claus, L.A.N., Leslie, M.E., Tao, K., Wu, Z., Liu, J., Yu, X., Li, B., Zhou, J., Savatin, D.V., et al. (2020). Ligand-induced monoubiquitination of BIK1 regulates plant immunity. Nature *581*, 199–203.

Masachis, S., Segorbe, D., Turrà, D., Leon-Ruiz, M., Fürst, U., El Ghalid, M., Leonard, G., López-Berges, M.S., Richards, T.A., Felix, G., et al. (2016). A fungal pathogen secretes plant alkalinizing peptides to increase infection. Nat Microbiol *1*, 16043.

Menna, A., Fischer-Stettler, M., Pfister, B., Andrés, G.S., Holbrook-Smith, D., and Sánchez-Rodríguez, C. (2020). Single-run HPLC Quantification of Plant Cell Wall Monosaccharides. Bio Protoc *10*, e3546.

Menna, A., Dora, S., Sancho-Andrés, G., Kashyap, A., Meena, M.K., Sklodowski, K., Gasperini, D., Coll, N.S., and Sánchez-Rodríguez, C. (2021). A primary cell wall cellulose-dependent defense mechanism against vascular pathogens revealed by time-resolved dual transcriptomics. BMC Biol. *19*, 1–20.

Mohnen, D. (2008). Pectin structure and biosynthesis. Curr. Opin. Plant Biol. *11*, 266–277.

Mort, A.J., Moerschbacher, B.M., Pierce, M.L., and Maness, N.O. (1991). Problems encountered during the extraction, purification, and chromatography of pectic fragments, and some solutions to them. Carbohydr. Res. *215*, 219–227.

Nagaya, S., Kawamura, K., Shinmyo, A., and Kato, K. (2010). The HSP terminator of Arabidopsis thaliana increases gene expression in plant cells. Plant Cell Physiol. *51*, 328–

332.

Nakagami, H., Pitzschke, A., and Hirt, H. (2005). Emerging MAP kinase pathways in plant stress signalling. Trends Plant Sci. *10*, 339–346.

Ortiz-Morea, F.A., Savatin, D.V., Dejonghe, W., Kumar, R., Luo, Y., Adamowski, M., Van den Begin, J., Dressano, K., Pereira de Oliveira, G., Zhao, X., et al. (2016). Danger-associated peptide signaling in Arabidopsis requires clathrin. Proc. Natl. Acad. Sci. U. S. A. *113*, 11028–11033.

Pan, X., Fang, L., Liu, J., Senay-Aras, B., Lin, W., Zheng, S., Zhang, T., Guo, J., Manor, U., Van Norman, J., et al. (2020). Auxin-induced signaling protein nanoclustering contributes to cell polarity formation. Nat. Commun. *11*, 3914.

Poncini, L., Wyrsch, I., Dénervaud Tendon, V., Vorley, T., Boller, T., Geldner, N., Métraux, J.-P., and Lehmann, S. (2017). In roots of Arabidopsis thaliana, the damage-associated molecular pattern AtPep1 is a stronger elicitor of immune signalling than flg22 or the chitin heptamer. PLoS One *12*, e0185808.

Qi, H., Zhu, X., Guo, F., Lv, L., and Zhang, Z. (2021). The Wall-Associated Receptor-Like Kinase TaWAK7D Is Required for Defense Responses to Rhizoctonia cerealis in Wheat. Int. J. Mol. Sci. *22*.

Ren, D., Liu, Y., Yang, K.-Y., Han, L., Mao, G., Glazebrook, J., and Zhang, S. (2008). A fungal-responsive MAPK cascade regulates phytoalexin biosynthesis in Arabidopsis. Proc. Natl. Acad. Sci. U. S. A. *105*, 5638–5643.

Ringli, C. (2010). Monitoring the outside: cell wall-sensing mechanisms. Plant Physiol. *153*, 1445–1452.

Rosli, H.G., Zheng, Y., Pombo, M.A., Zhong, S., Bombarely, A., Fei, Z., Collmer, A., and Martin, G.B. (2013). Transcriptomics-based screen for genes induced by flagellin and repressed by pathogen effectors identifies a cell wall-associated kinase involved in plant immunity. Genome Biol. *14*, R139.

Safran, J., Habrylo, O., Cherkaoui, M., Lecomte, S., Voxeur, A., Pilard, S., Bassard, S., Pau-Roblot, C., Mercadante, D., Pelloux, J., et al. (2021). New insights into the specificity and processivity of two novel pectinases from Verticillium dahliae. Int. J. Biol. Macromol. *176*, 165–176.

Saintenac, C., Lee, W.-S., Cambon, F., Rudd, J.J., King, R.C., Marande, W., Powers, S.J., Bergès, H., Phillips, A.L., Uauy, C., et al. (2018). Wheat receptor-kinase-like protein Stb6 controls gene-for-gene resistance to fungal pathogen Zymoseptoria tritici. Nat. Genet. *50*, 368–374.

Schindelin, J., Arganda-Carreras, I., Frise, E., Kaynig, V., Longair, M., Pietzsch, T., Preibisch, S., Rueden, C., Saalfeld, S., Schmid, B., et al. (2012). Fiji: an open-source platform for biological-image analysis. Nat. Methods *9*, 676–682.

Schmittgen, T.D., and Livak, K.J. (2008). Analyzing real-time PCR data by the comparative C(T) method. Nat. Protoc. *3*, 1101–1108.

Schwessinger, B., Roux, M., Kadota, Y., Ntoukakis, V., Sklenar, J., Jones, A., and Zipfel, C. (2011). Phosphorylation-dependent differential regulation of plant growth, cell death, and innate immunity by the regulatory receptor-like kinase BAK1. PLoS Genet. *7*, e1002046.

Shimada, Y., Goda, H., Nakamura, A., Takatsuto, S., Fujioka, S., and Yoshida, S. (2003). Organ-Specific Expression of Brassinosteroid-Biosynthetic Genes and Distribution of Endogenous Brassinosteroids in Arabidopsis. Plant Physiology *131*, 287–297.

Souza, C. de A., Li, S., Lin, A.Z., Boutrot, F., Grossmann, G., Zipfel, C., and Somerville, S.C. (2017). Cellulose-Derived Oligomers Act as Damage-Associated Molecular Patterns and Trigger Defense-Like Responses. Plant Physiol. *173*, 2383–2398.

Thevenaz, P., Ruttimann, U.E., and Unser, M. (1998). A pyramid approach to subpixel registration based on intensity. IEEE Trans. Image Process. *7*, 27–41.

Tinevez, J.-Y., Perry, N., Schindelin, J., Hoopes, G.M., Reynolds, G.D., Laplantine, E., Bednarek, S.Y., Shorte, S.L., and Eliceiri, K.W. (2017). TrackMate: An open and extensible platform for single-particle tracking. Methods *115*, 80–90.

Vaahtera, L., Schulz, J., and Hamann, T. (2019). Cell wall integrity maintenance during plant development and interaction with the environment. Nat Plants *5*, 924–932.

Verica, J.A., and He, Z.-H. (2002). The cell wall-associated kinase (WAK) and WAK-like kinase gene family. Plant Physiol. *129*, 455–459.

Verica, J.A., Chae, L., Tong, H., Ingmire, P., and He, Z.-H. (2003). Tissue-specific and developmentally regulated expression of a cluster of tandemly arrayed cell wall-associated kinase-like kinase genes in Arabidopsis. Plant Physiol. *133*, 1732–1746.

Wagner, T.A., and Kohorn, B.D. (2001). Wall-associated kinases are expressed throughout plant development and are required for cell expansion. Plant Cell *13*, 303–318.

Wagner, T., Kroll, A., Haramagatti, C.R., Lipinski, H.-G., and Wiemann, M. (2017). Classification and Segmentation of Nanoparticle Diffusion Trajectories in Cellular Micro Environments. PLoS One *12*, e0170165.

Wang, P., Zhou, L., Jamieson, P., Zhang, L., Zhao, Z., Babilonia, K., Shao, W., Wu, L., Mustafa, R., Amin, I., et al. (2020). The Cotton Wall-Associated Kinase GhWAK7A Mediates Responses to Fungal Wilt Pathogens by Complexing with the Chitin Sensory Receptors. Plant Cell *32*, 3978–4001.

Wojtasik, W., Kulma, A., Kostyn, K., and Szopa, J. (2011). The changes in pectin metabolism in flax infected with Fusarium. Plant Physiol. Biochem. *49*, 862–872.

Wolf, S., Mravec, J., Greiner, S., Mouille, G., and Höfte, H. (2012). Plant cell wall homeostasis is mediated by brassinosteroid feedback signaling. Curr. Biol. *22*, 1732–1737.

Wolf, S., van der Does, D., Ladwig, F., Sticht, C., Kolbeck, A., Schürholz, A.-K., Augustin, S., Keinath, N., Rausch, T., Greiner, S., et al. (2014). A receptor-like protein mediates the response to pectin modification by activating brassinosteroid signaling. Proc. Natl. Acad. Sci. U. S. A. *111*, 15261–15266.

Wormit, A., and Usadel, B. (2018). The Multifaceted Role of Pectin Methylesterase Inhibitors (PMEIs). Int. J. Mol. Sci. *19*.

Wu, X., Bacic, A., Johnson, K.L., and Humphries, J. (2020). The Role of Brachypodium distachyon Wall-Associated Kinases (WAKs) in Cell Expansion and Stress Responses. Cells *9*.

Xu, W., Huang, J., Li, B., Li, J., and Wang, Y. (2008). Is kinase activity essential for biological functions of BRI1? Cell Res. *18*, 472–478.

Yang, J., Xie, M., Wang, X., Wang, G., Zhang, Y., Li, Z., and Ma, Z. (2021). Identification of cell wall-associated kinases as important regulators involved in Gossypium hirsutum resistance to Verticillium dahliae. BMC Plant Biol. *21*, 220.

Yang, Y., Zhang, Y., Li, B., Yang, X., Dong, Y., and Qiu, D. (2018). A Verticillium dahliae Pectate Lyase Induces Plant Immune Responses and Contributes to Virulence. Front. Plant Sci. *9*, 1271.

Zhang, N., Pombo, M.A., Rosli, H.G., and Martin, G.B. (2020). Tomato Wall-Associated Kinase SlWak1 Depends on Fls2/Fls3 to Promote Apoplastic Immune Responses to Pseudomonas syringae. Plant Physiol. *183*, 1869–1882.

Zhou, J., Liu, D., Wang, P., Ma, X., Lin, W., Chen, S., Mishev, K., Lu, D., Kumar, R., Vanhoutte, I., et al. (2018). Regulation of Arabidopsis brassinosteroid receptor BRI1 endocytosis and degradation by plant U-box PUB12/PUB13-mediated ubiquitination. Proc. Natl. Acad. Sci. U. S. A. *115*, E1906–E1915.

Zhou, N., Tootle, T.L., Tsui, F., Klessig, D.F., and Glazebrook, J. (1998). PAD4 functions upstream from salicylic acid to control defense responses in Arabidopsis. Plant Cell *10*, 1021–1030.

Figure 1

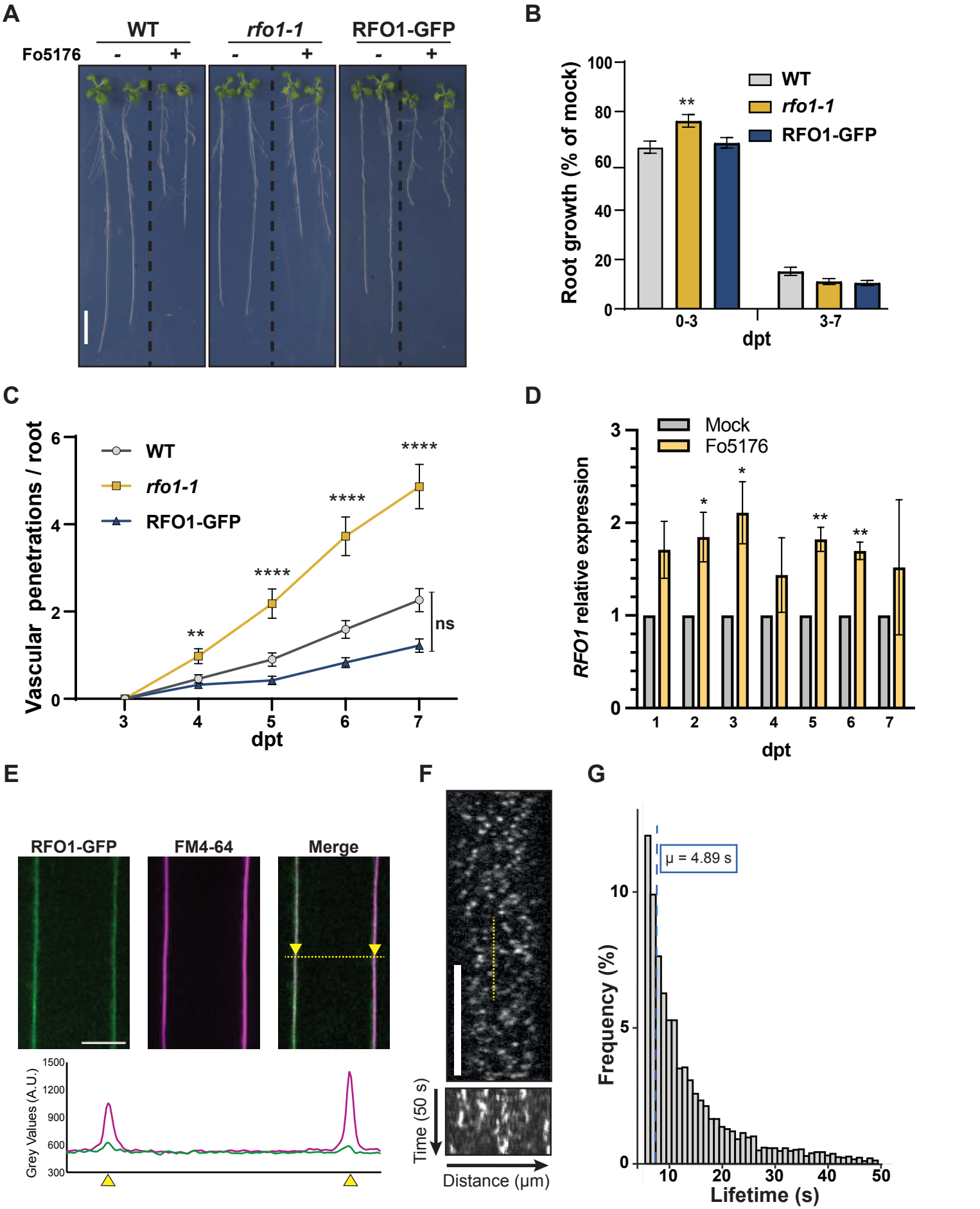
A
WT
rfo1-1
RFO1-GFP
Fo5176
- + - + - +
B
Root growth (% of mock)
100
80
60
40
20
0
**
WT
rfo1-1
RFO1-GFP
0-3
3-7
dpt
C
Vascular penetrations / root
6
4
2
0
WT
rfo1-1
RFO1-GFP
**
****
****
****
ns
3
4
5
6
7
dpt
D
RFO1 relative expression
3
2
1
0
Mock
Fo5176
*
*
**
**
1
2
3
4
5
6
7
dpt
E
RFO1-GFP
FM4-64
Merge
Grey Values (A.U.)
1500
1200
900
600
300
F
Time (50 s)
Distance (µm)
G
Frequency (%)
10
5
0
µ = 4.89 s
10
20
30
40
50
Lifetime (s)

Figure 2

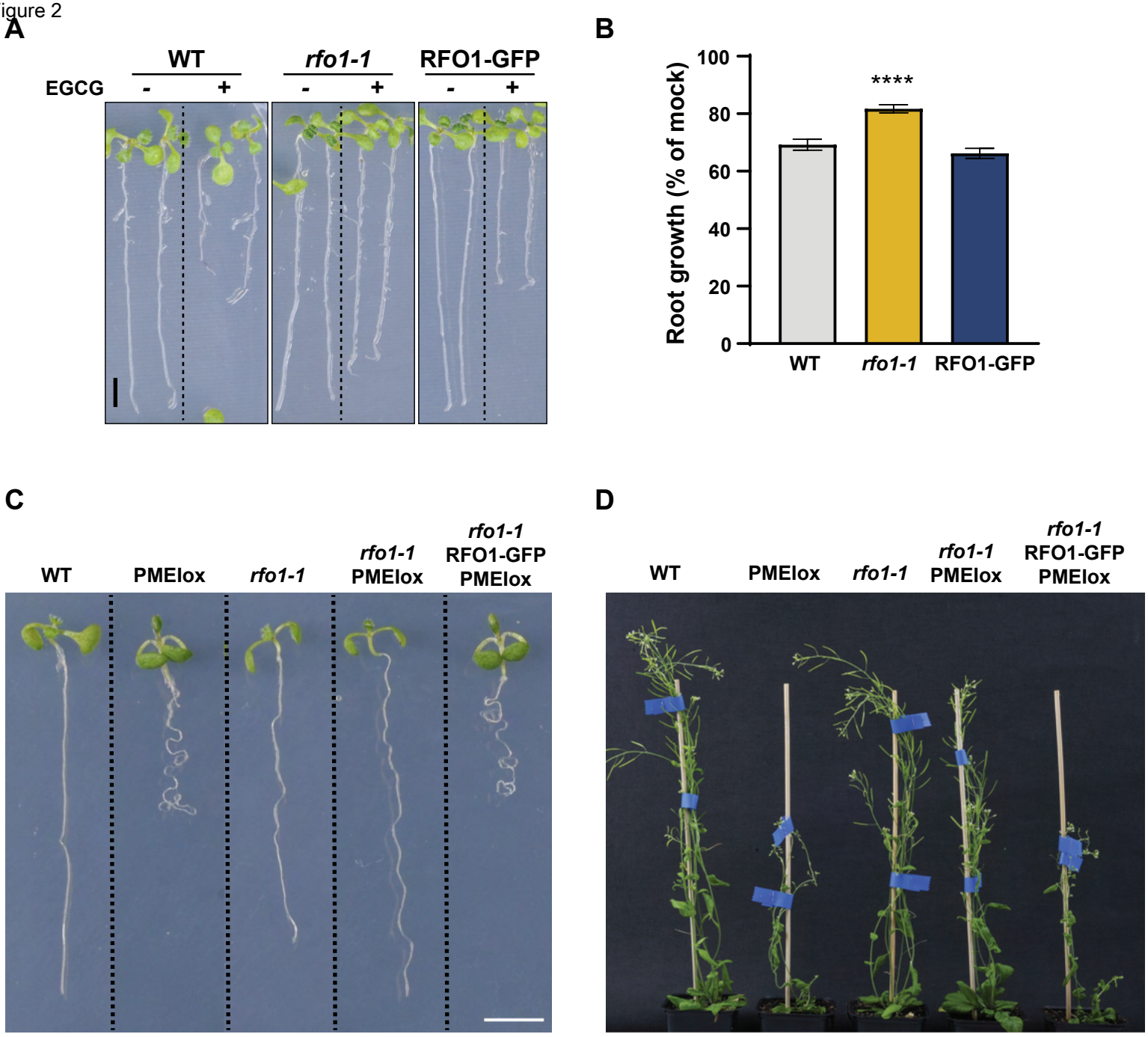
A
WT
rfo1-1
RFO1-GFP
EGCG
- + - + - +
B
Root growth (% of mock)
100
80
60
40
20
0
****
WT
rfo1-1
RFO1-GFP
C
WT
PMEIox
rfo1-1
rfo1-1 PMEIox
rfo1-1 RFO1-GFP PMEIox
D
WT
PMEIox
rfo1-1
rfo1-1 PMEIox
rfo1-1 RFO1-GFP PMEIox

Figure 3

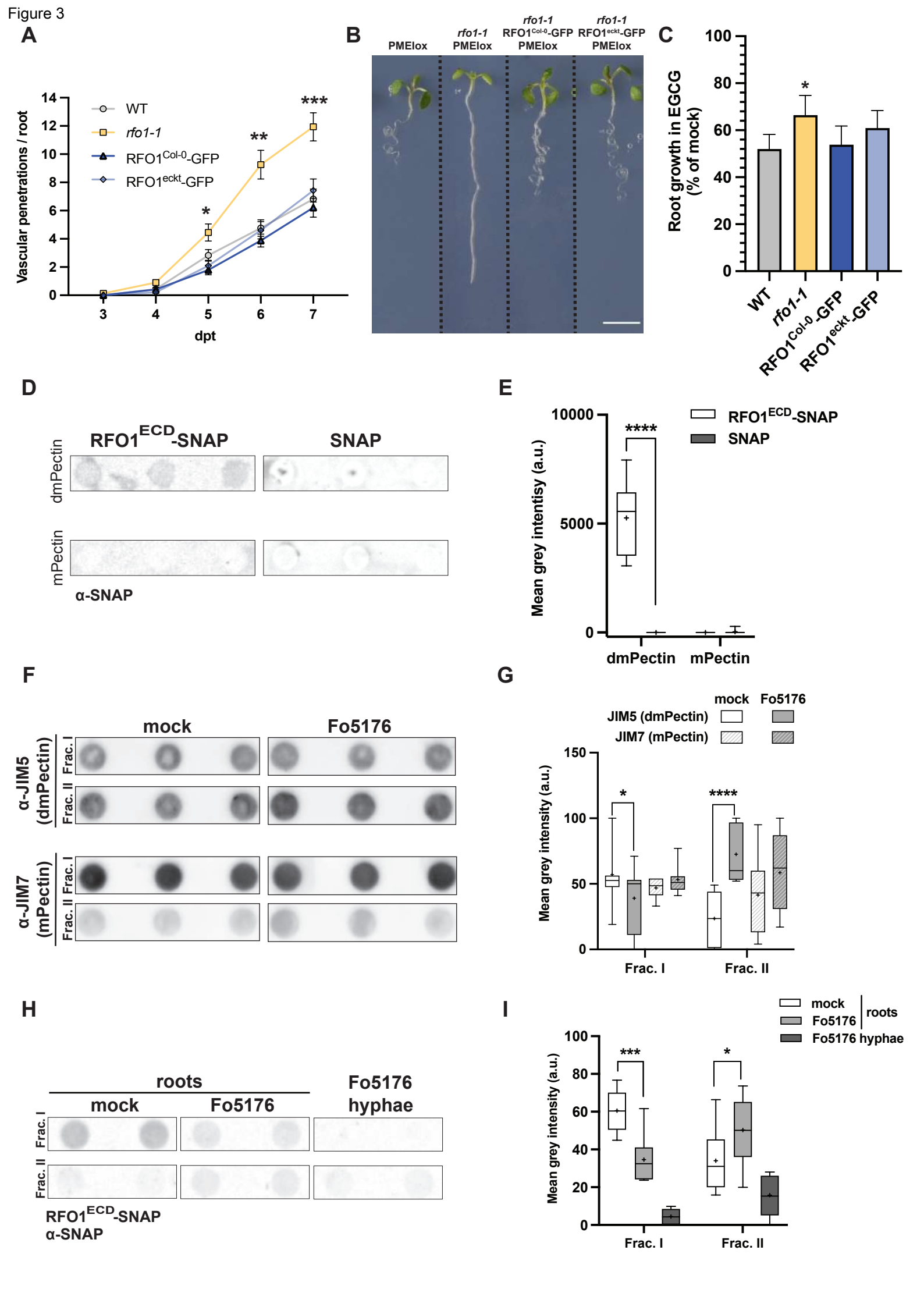
A
Vascular penetrations / root
dpt
WT
rfo1-1
RFO1Col-0-GFP
RFO1eckt-GFP
B
PMEIox
rfo1-1 PMEIox
rfo1-1 RFO1Col-0-GFP PMEIox
rfo1-1 RFO1eckt-GFP PMEIox
C
Root growth in EGCG (% of mock)
WT
rfo1-1
RFO1Col-0-GFP
RFO1eckt-GFP
D
RFO1ECD-SNAP
SNAP
dmPectin
mPectin
α-SNAP
E
RFO1ECD-SNAP
SNAP
Mean grey intentisy (a.u.)
dmPectin
mPectin
F
mock
Fo5176
α-JIM5 (dmPectin)
α-JIM7 (mPectin)
Frac. I
Frac. II
G
mock
Fo5176
JIM5 (dmPectin)
JIM7 (mPectin)
Mean grey intensity (a.u.)
Frac. I
Frac. II
H
roots
mock
Fo5176
Fo5176 hyphae
Frac. I
Frac. II
RFO1ECD-SNAP
α-SNAP
I
mock
Fo5176
roots
Fo5176 hyphae
Mean grey intensity (a.u.)
Frac. I
Frac. II

Figure 4

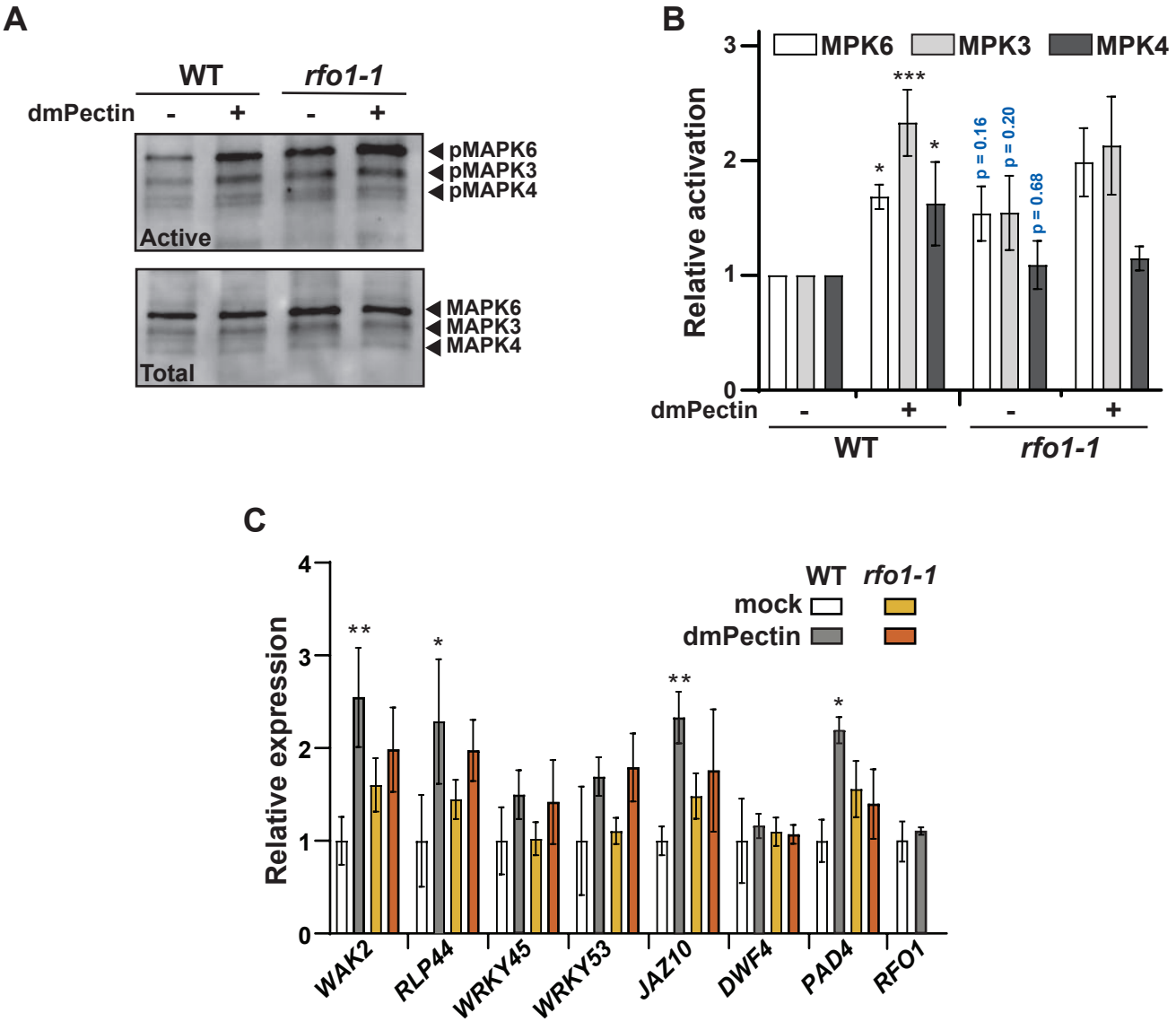
A
WT
rfo1-1
dmPectin - + - +
pMAPK6
pMAPK3
pMAPK4
Active
MAPK6
MAPK3
MAPK4
Total
B
MPK6
MPK3
MPK4
Relative activation
dmPectin - + - +
WT
rfo1-1
p = 0.16
p = 0.20
p = 0.68
C
WT
rfo1-1
mock
dmPectin
Relative expression
WAK2
RLP44
WRKY45
WRKY53
JAZ10
DWF4
PAD4
RFO1

Figure 5

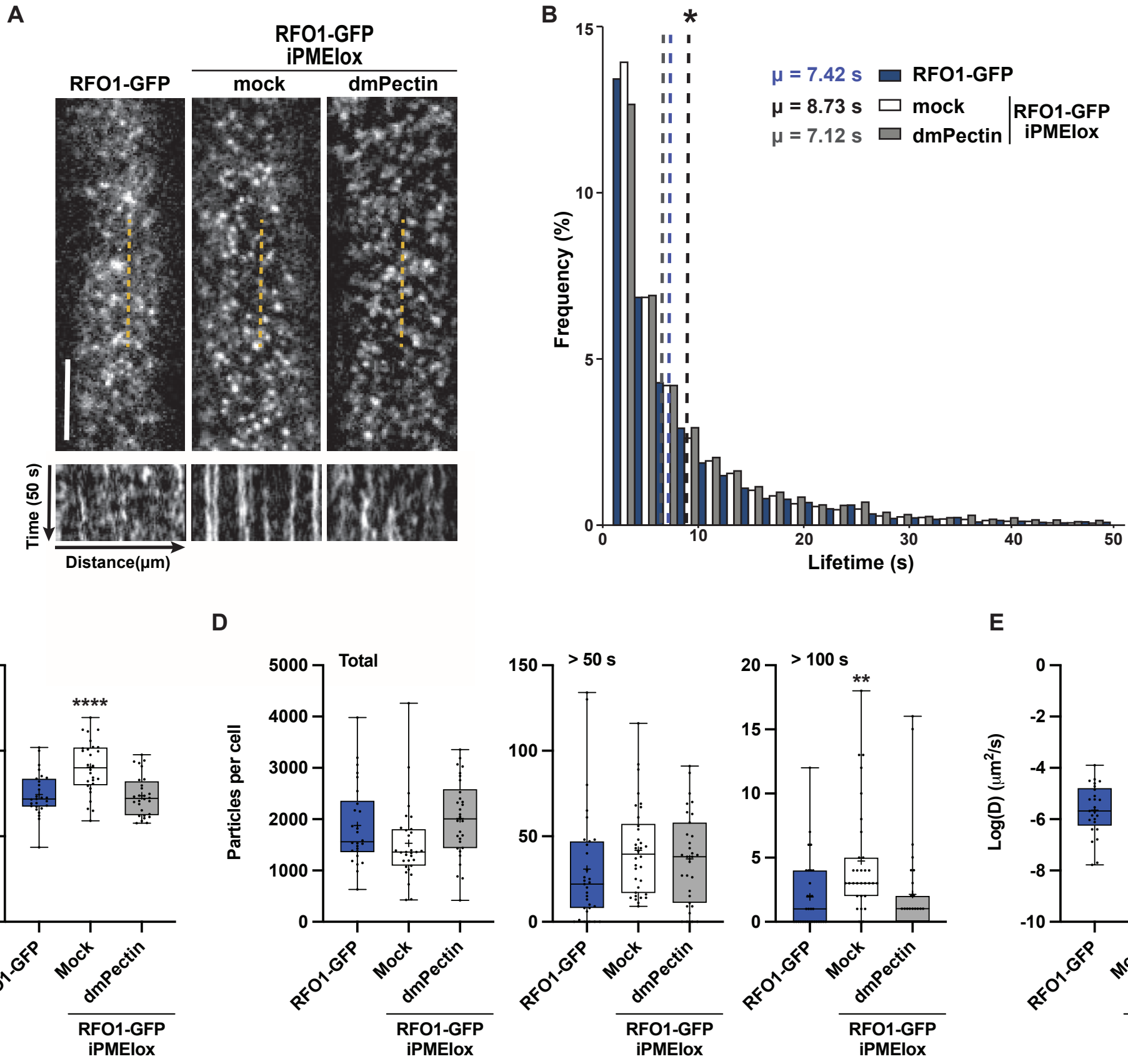
A
RFO1-GFP
iPMElox
RFO1-GFP
mock
dmPectin
Time (50 s)
Distance(µm)
B
Frequency (%)
Lifetime (s)
µ = 7.42 s
µ = 8.73 s
µ = 7.12 s
RFO1-GFP
mock
dmPectin
RFO1-GFP
iPMElox
C
Lifetime (s)
****
D
Total
Particles per cell
> 50 s
> 100 s
**
E
Log(D) (µm²/s)
RFO1-GFP
Mock
dmPectin
RFO1-GFP
iPMElox

Figure 6

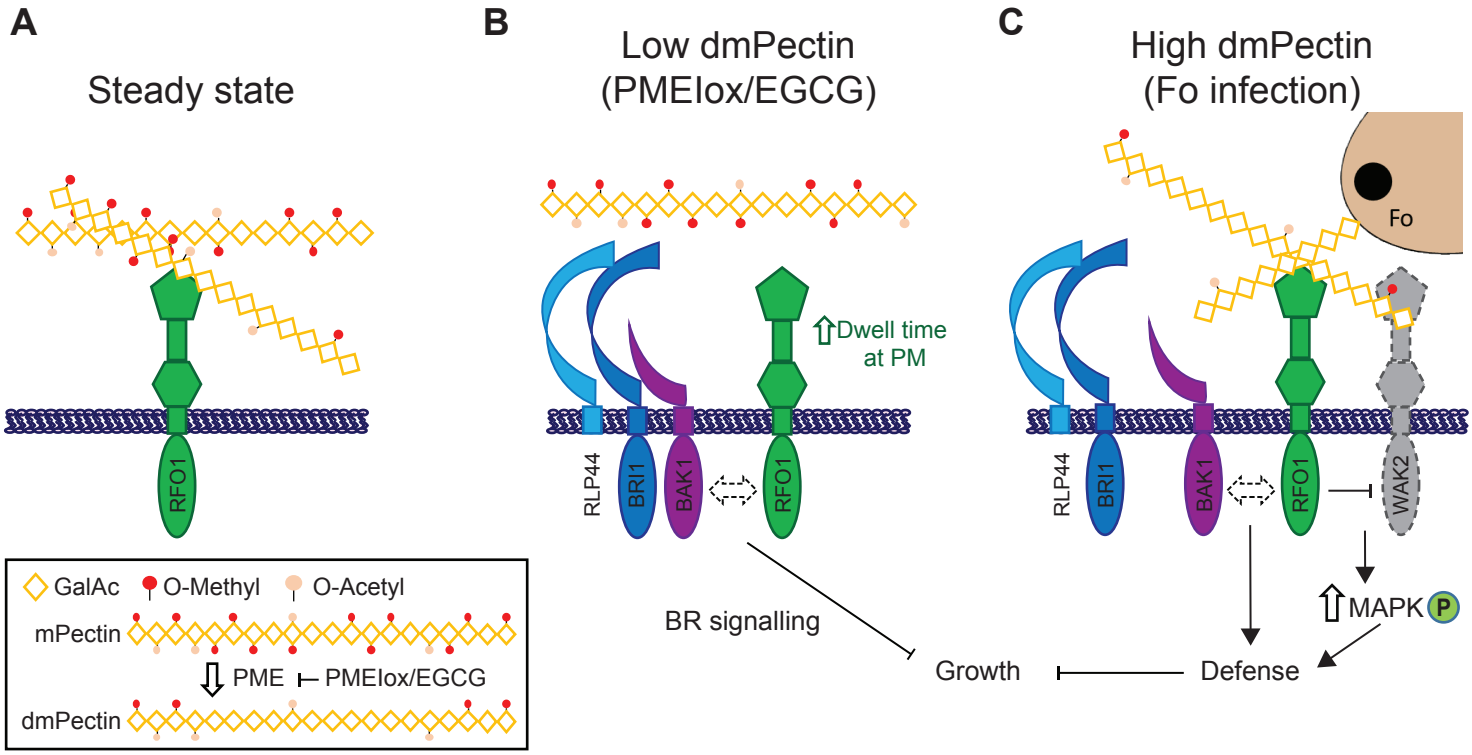
A
Steady state
RFO1
GalAc
O-Methyl
O-Acetyl
mPectin
PME
PMEIox/EGCG
dmPectin
B
Low dmPectin
(PMEIox/EGCG)
Dwell time
at PM
RLP44
BRI1
BAK1
RFO1
BR signalling
Growth
C
High dmPectin
(Fo infection)
Fo
RLP44
BRI1
BAK1
RFO1
WAK2
MAPK
P
Defense

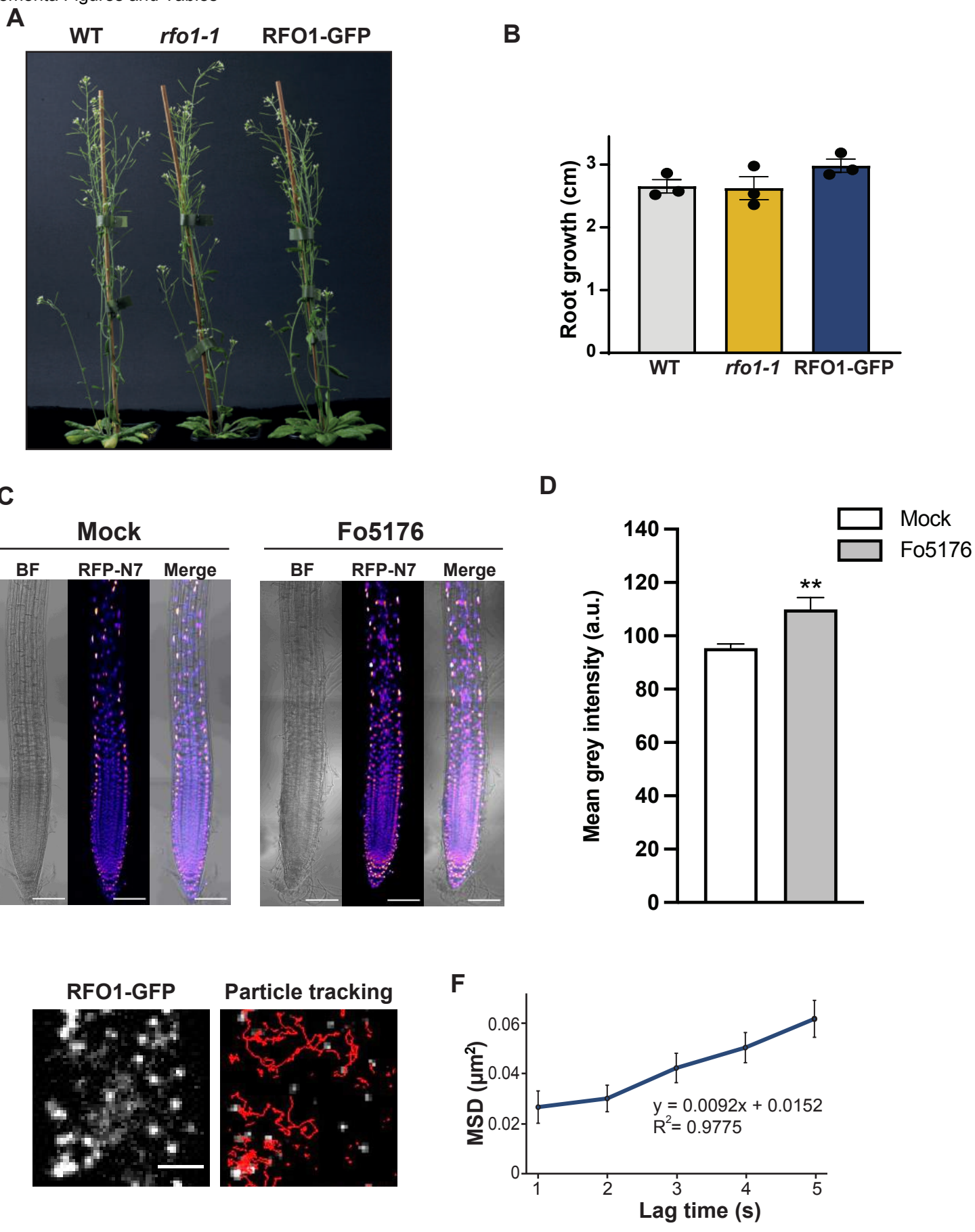
A
WT
rfo1-1
RFO1-GFP
B
Root growth (cm)
0
1
2
3
WT
rfo1-1
RFO1-GFP
C
Mock
Fo5176
BF
RFP-N7
Merge
BF
RFP-N7
Merge
D
Mock
Fo5176
Mean grey intensity (a.u.)
0
20
40
60
80
100
120
140
**
E
RFO1-GFP
Particle tracking
F
MSD (μm²)
0
0.02
0.04
0.06
y = 0.0092x + 0.0152
R²= 0.9775
1
2
3
4
5
Lag time (s)

Figure S1. Growth phenotypes and in vivo RFO1-GFP dynamics at the PM. Related to Figure 1.

(A) Representative image of 8-week old wild type (WT, Col-0), rfo1-1, and RFO1-GFP (rfo1-1 pRFO1::RFO1-GFP) plants. **(B)** Root growth of 8-day old WT, rfo1-1, and RFO1-GFP seedlings after 3 dpt to mock plates. Data represents the mean ±SE of >30 seedlings per genotype from 3 independent replicates with a minimum of 10 seedlings per replicate. Two-way ANOVA with Dunnett's multiple comparison test, no significance observed. **(C)** Representative brightfield (BF) and fluorescence images of nuclear RFP from pRFO1::RFP-N7 roots at 2 dpt to mock or Fo5176 pSIX1::GFP containing plates. Scale bar = 100 µm. **(D)** Quantification of the RFP signal intensity (a.u.) in epidermal cells of the root tip in roots as in (C). N ≥ 750 cells from 30 roots for mock and 684 cells from 30 roots for Fo5176 in 3 independent replicates. Unpaired t-test, p-value **<0.01. **(E)** Representative spinning disc confocal image of RFO1-GFP particles at the PM of a 5-day old root elongating epidermal cell (left) with particle tracks shown in red after single-particle tracking with Trackmate (right). Scale bar = 5 µm. **(F)** Means squared displacement (MSD) plot of RFO1-GFP particles at the PM as shown in (D) with a linear fit, derived equation, and R2 value.

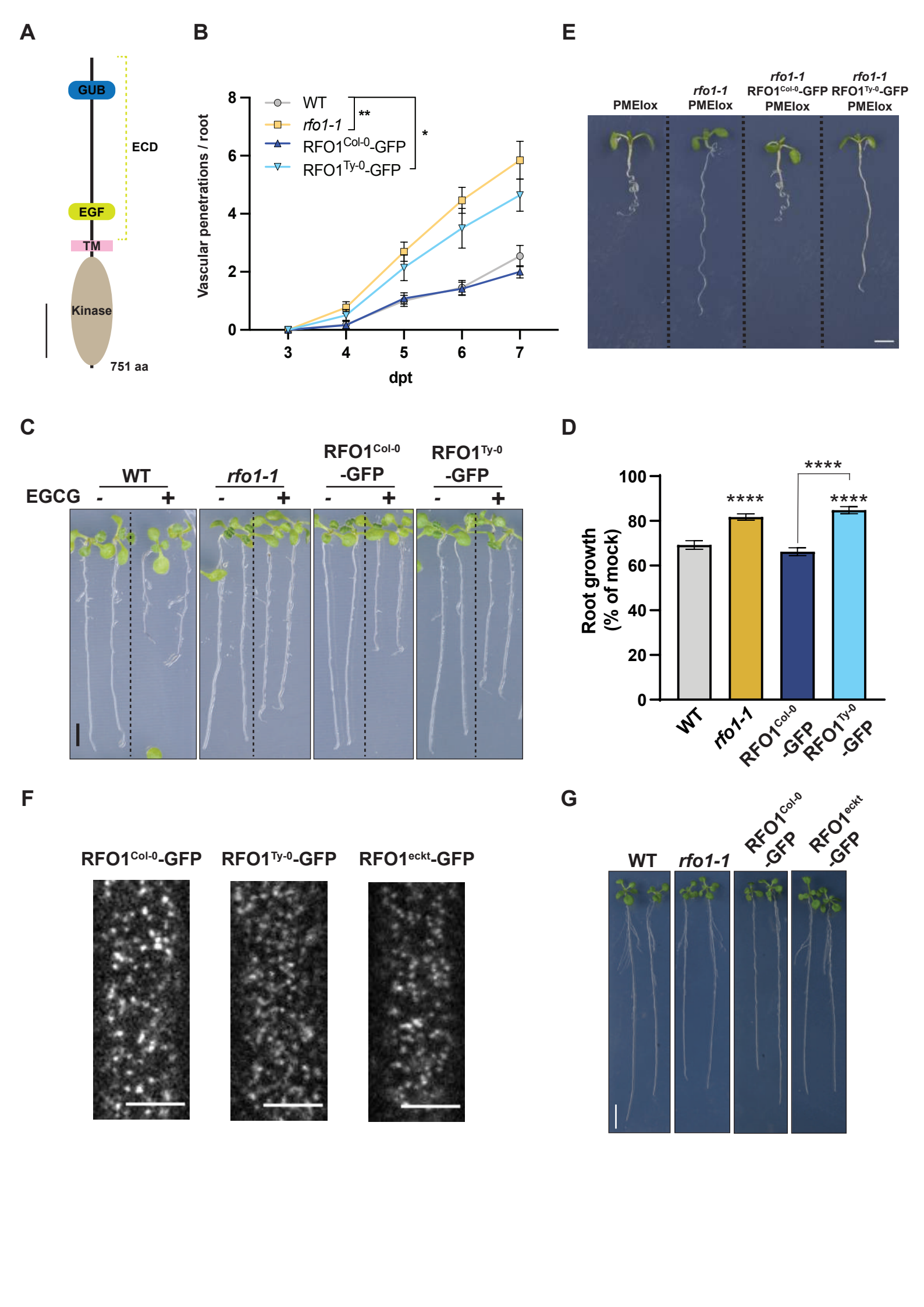
A
GUB
ECD
EGF
TM
Kinase
751 aa
B
Vascular penetrations / root
WT
rfo1-1
RFO1Col-0-GFP
RFO1Ty-0-GFP
**
*
dpt
E
PMEIox
rfo1-1 PMEIox
rfo1-1 RFO1Col-0-GFP PMEIox
rfo1-1 RFO1Ty-0-GFP PMEIox
C
EGCG
WT
rfo1-1
RFO1Col-0 -GFP
RFO1Ty-0 -GFP
D
Root growth (% of mock)
****
F
RFO1Col-0-GFP
RFO1Ty-0-GFP
RFO1eckt-GFP
G
WT
rfo1-1
RFO1Col-0 -GFP
RFO1eckt -GFP

Figure S2. The plasma membrane localized RFO1^{Ty-0}-GFP does not play a significant role in plant defense against Fo5176 or response to EGCG-induced pectin perturbations. Related to Figure 2.

(A) Scheme of *in silico* predicted protein structure of RFO1 using the Plant Proteome Database (PPDB, http://ppdb.tc.cornell.edu/default.aspx). GUB, galacturonan-binding domain. EGF, calcium binding domain. TM, Transmembrane domain. ECD, Extracellular domain. Scale bar = 100 amino acids (aa). **(B)** Cumulative vascular penetrations observed in wild type (WT; Col-0), *rfo1-1*, RFO1^{Col-0}-GFP (*rfo1-1* pRFO1::RFO1^{Col-0}-GFP), and RFO1^{Ty-0}-GFP (*rfo1-1* pRFO1::RFO1^{Ty-0}-GFP) roots between 3 and 7 dpt to plates containing Fo5176 pSIX1::GFP microconidia. Data represents the mean ± SE of N ≥ 10 seedlings per genotype from 3 independent replicates. RM ANOVA with Tukey's multi-comparison post-hoc test, p-values *< 0.05, **<0.01. Significance shown compared to WT. **(C)** Representative image of 8-day old WT, *rfo1-1*, RFO1^{Col-0}-GFP, and RFO1^{Ty-0}-GFP seedlings after 48 hours upon mock (-) or 6.25 µM EGCG (+) treatment. Scale bar = 5mm. **(D)** Root growth of EGCG-treated roots relative to mock-treated ones (%), as shown in (B). Bars represent the mean ± SE of >38 seedlings per genotype from 4 independent replicates. One-way ANOVA with Dunnett's multiple-comparison post-hoc test, p-value ****<0.0001. Significance shown compared to WT unless indicated. **(E)** Representative images of 8-day old WT, PMEIox, *rfo1-1*, *rfo1-1* PMEIox, *rfo1-1* RFO1^{Col-0}-GFP PMEIox, and *rfo1-1* RFO1^{Ty-0}-GFP PMEIox seedlings. Scale bar = 5 mm. **(F)** Representative spinning disc confocal image of RFO1^{Col-0}-GFP, RFO1^{Ty-0}-GFP and RFO1^{eckt0}-GFP particles at the PM of 5 days-old root epidermal cells. Scale bar = 5 µm. **(G)** Representative images of 11-day old WT, *rfo1-1*, RFO1^{Col-0}-GFP, and RFO1^{eckt}-GFP seedlings. Scale bar = 10 mm.

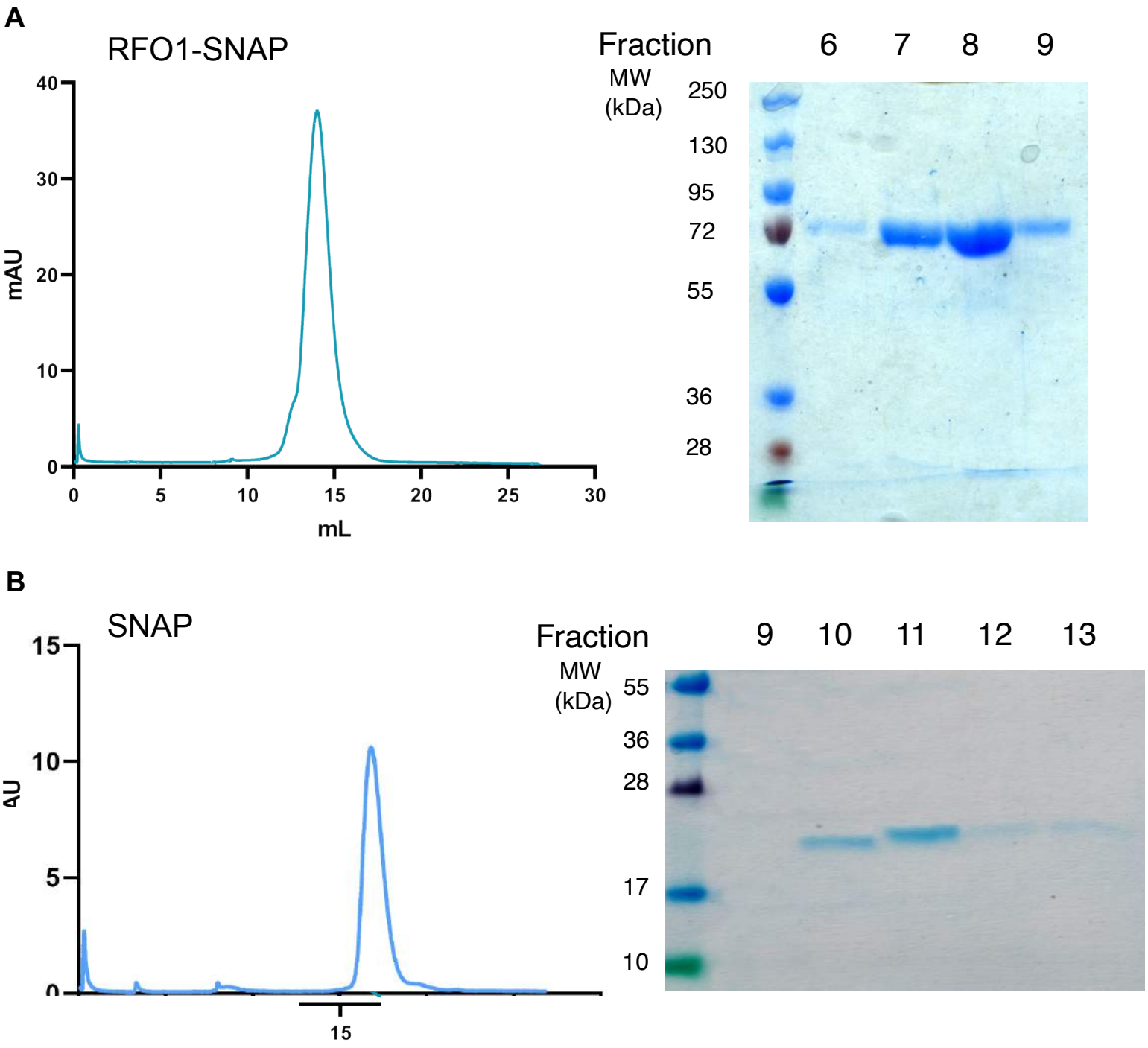

Figure S3. Size exclusion and SDS-PAGE analysis of RFO1^{ECD}-SNAP and SNAP recombinant proteins from insect cells. Related to Figure 3.

(A) Size exclusion chromatography (SEC, left) of RFO1^{ECD}-SNAP protein and SDS-PAGE (right) of the different fractions corresponding to the SEC elution peak. **(B)** Size exclusion chromatography (SEC, left) of SNAP and SDS-PAGE (right) of the different fractions of the SEC experiment.

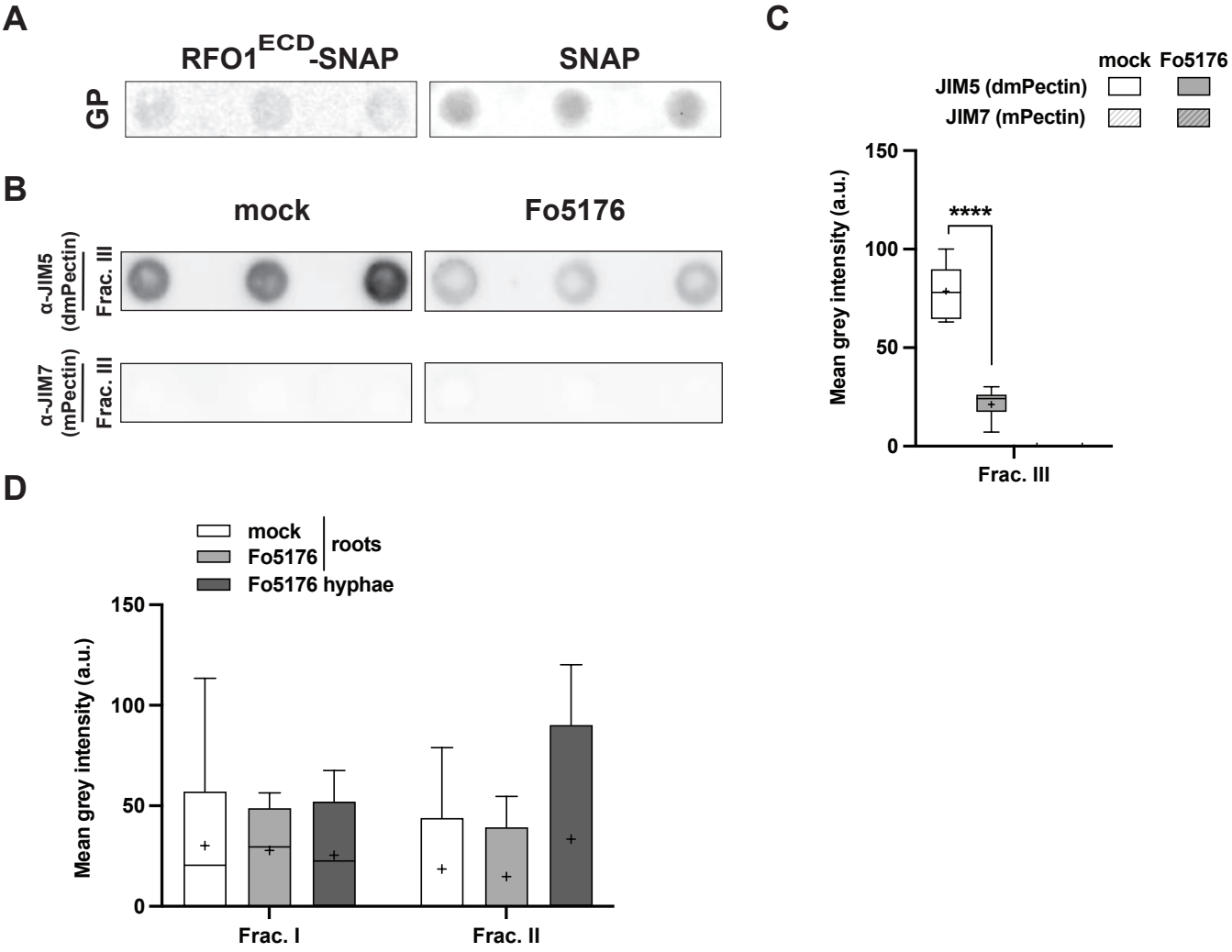

Figure S4. Dot immunobinding assays using plant glycoprotein extracts and cell wall fractions. Related to Figure 3.

(A) Representative dot immunobinding assays using plant CW glycoprotein (GP) extracts probed with RFO1^{ECD}-SNAP or SNAP proteins. The experiment was repeated three times with similar results. **(B)** Representative dot immunobinding assay of immobilized plant CW fraction III from mock and Fo5176-infected WT roots at 4dpt and probed with JIM5 or JIM7 antibodies. **(C)** Quantification of dot immunobinding assays intensities as a percent of mean gray values from blots as depicted in (B). **(D)** Quantification of dot immunobinding assays intensities as a percent of mean gray values per CW fraction probed with SNAP, as shown in (D). Box plots: centerlines show the medians; means marked by +; box limits indicate the 25th and 75th percentiles; whiskers extend to the minimum and maximum. N=3 independent replicates. Two-way ANOVA with Tukey's multiple comparison test, no significance observed.

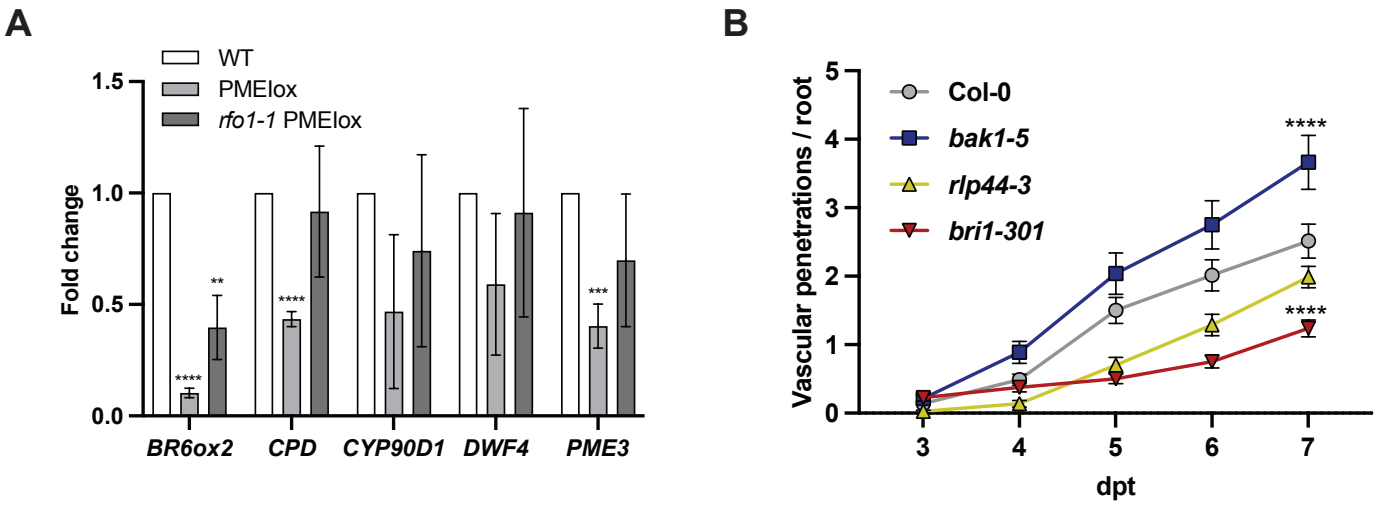

Figure S5. RFO1 activates BR signaling, which participates in defense against Fo. *bri1-301 but not rlp44-3* mutant is more resistant than wild type to Fo5176 vasculature colonization.

(A) *BR6ox2*, *CPD*, *CYP90D1*, *DWF4* and *PME3* gene expression relative to *GAPDH*, in 8 days-old WT, PMEIox and *rfo1-1* PMEIox plants, normalized to mock WT gene expression. Data represents the mean ±SE of N = 3 independent replicates. Unpaired *t*-test (two-tailed) against WT mock per gene, p-values *< 0.05, **<0.01. **(B)** Cumulative vascular penetration of Fo5176 per root of wild type (WT; Col-0), *rlp44-3*, *bri1-301,* and *bak1-5* at different days post-transfer (dpt) to Fo5176 pSIX1::GFP microconidia-containing plates. Data represents the mean ± SE of N > 30 seedlings per genotype from three independent biological replicates. Two-way ANOVA with Tukey's multiple comparison test, p-value **** < 0.0001 at 7dpt. See Table S1 the complete statistical analysis.

Table S1. Statistical analysis of root vascular penetrations upon Fo5176 pSIX1::GFP infection. Related to Figure S5.

Statistical analysis of root vascular penetrations upon Fo5176 pSIX1::GFP infection. Two-way ANOVA with post-hoc Tukey test for multiple comparisons corresponding to root vascular penetration events (p-value < 0.05 *, 0.01 **, 0.001 ***, 0.0001 ****). Day 3 post treatment is not included because there were no statistically significant differences (p-value > 0.05).

Two-way ANOVA (Tukey test)	**Adjusted p-value**
4 dpt	
WT vs. *bak1-5*	ns
WT vs. *rlp44-3*	ns
WT vs. *bri1-301*	ns
bak1-5 vs. *rlp44-3*	*
bak1-5 vs. *bri1-301*	ns
rlp44-3 vs. *bri1-301*	ns
5 dpt	
WT vs. *bak1-5*	ns
WT vs. *rlp44-3*	**
WT vs. *bri1-301*	***
bak1-5 vs. *rlp44-3*	****
bak1-5 vs. *bri1-301*	****
rlp44-3 vs. *bri1-301*	ns
6 dpt	
WT vs. *bak1-5*	*
WT vs. *rlp44-3*	*
WT vs. *bri1-301*	****
bak1-5 vs. *rlp44-3*	****
bak1-5 vs. *bri1-301*	****
rlp44-3 vs. *bri1-301*	ns
7 dpt	
WT vs. *bak1-5*	****
WT vs. *rlp44-3*	ns
WT vs. *bri1-301*	****
bak1-5 vs. *rlp44-3*	****

bak1-5 vs. *bri1-301*	****
rlp44-3 vs. *bri1-301*	*

Table S2. Primers used in this work.

		NAME	SEQUENCE	#
CLONING	pRFO1:RFO1-GFP pRFO1:RFO1^{Ty-0}-GFP pRFO1:RFO1^{eckt}-GFP	pRFO1_FW	CATGATTACGAATTCGAGCTCCGTCGCGGTCAGATGTTGAAC	1
		pRFO1_RV	CTTAGAGGATCCCGCACTCGAGGCCGTCTCGTTGGAATTTGGAAG	2
		RFO1_FW	CACCATGAAGAGAAGGAGACTTTTTTTCTC	3
		RFO1_RV	CCATGTTCGTTGAGGAACCAGC	4
		RFO1_TY_FW	CACCATGAAGAGAAGGAGACTTTTTTTCTTGT	5
		RFO1_TM_FW	GTTCTAGGTTTTCCACTGTTGTTCTT	6
		RFO1_TM_RV	AAGAACAACAGTGGAAAACCTAGAAC	7
	pRFO1::RFP-N7	pRFO1_N7_GFP_FW	CGAATTGGAGCTGCGGCCGCGAATTCCGTCGCGGTCAGATGTTGAAC	8
		pRFO1_N7_GFP_RV	CCTCGCCCTTGCTCACCATGCCGTCTCGTTGGAATTTGGAAG	9
		RFP_FW	ATGGTGAGCAAGGGCGAGG	10
		RFP_RV	GGCGCCCGCCGCCGCCGCCGCTCCCTTGTACAGCTCGTCCATGC	11
		N7_FW	GGAGCGGCGGCGGCGGCGGGCGCCGAATTCAAGCGTGAAGAGCAAGC	12
		N7_RV	TTTCATCTTCATCTTCATATTCTAGATCACTCTTCTTCTTGATCAGCTTCTGTGTCG	13
GENOTYPING	GFP	GFP_FW	ATCTTCTTCAAGGACGACGG	14
		GFP_RV	CTGTTGTAGTTGTACTCCAGCT	15
	PMEIox	attB1	GGGGACAAGTTTGTACAAAAAAGCAGGCT	16
		attB2	GGGGACCACTTTGTACAAGAAAGCTGGGT	17
	RFO1	SALK_077975 _LP	TACCAACCAAGCTCAATCACC	18
		SALK_077975 _RP	TATGAATGATTTGCGTTGGTG	19
		SALK_LB	CGCTTTCTTCCCTTCCTTTCTC	20
RT-PCR	BR6ox2	BR6ox2_FW	CAATAGTCTCAATGGACGCAGAGT	21
		BR6ox2_RV	AACCGCAGCTATGTTGCATG	22
	CPD	CPD_FW	CCCAAACCACTTCAAAGATGCT	23
		CPD_RV	GGGCCTGTCGTTACCGAGTT	24
	CYP90D1	CYP90D1_FW	CTCATTACCCTTGCCGTCAAA	25
		CYP90D1_RV	CAGCTTCATGTTTTCTTCCGTTAG	26
	DWF4	DWF4_FW	CAACAGCAAAACAACGGAGCG	27
		DWF4_RV	TCTGAACCAGCACATAGCCTTG	28
	GAPDH	GAPDH_FW	AGGTGGAAGAGCTGCTTCCTTC	29
		GAPDH_RV	GCAACACTTTCCCAACAGCCT	30
	JAZ10	JAZ10_FW	CGCCAGGTCTAGTACCGAAC	31
		JAZ10_RV	TGCTGCTTCATTAGCGACCT	32
	PAD4	PAD4_FW	CACCGCACTTTGGCTTCTATC	33
		PAD4_RV	AGTAAGTTCCAAAGGGCCAG	34
	PME3	PME3_FW	ACGGTAGCACCACTTTCCAC	35
		PME3_RV	ATCAGAACCCACACGGAGAG	36
	RFO1	RFO1_FW	ATGAAGAGAAGGAGACTTTTTTTCTCTGTTC	37
		RFO1_RV	ACCTCGTACCAGTCGTTGAG	38
	RLP44	RLP44_FW	TCAGATTCCGCAGCAATTAG	39
		RLP44_RV	TCCTGCAACGGATAACCATA	40
	WAK2	WAK2_FW	AACTGCCCATCTGGTTACCG	41
		WAK2_RV	CTCTGTGTTCTTCCGGTGCT	42
	WRKY45	WRKY45_FW	GGAGGGAAGATGTGCATTTGTG	43
		WRKY45_RV	GAACAATCCATTCCCCAGGAG	44
	WRKY53	WRKY53_FW	GCGACAAGACACCAGAGTCA	45
		WRKY53_RV	ACCGTTGGATTGAACCAGTC	46

Movie S1

Click here to access/download

Supplemental Videos and Spreadsheets

Movie S1.avi

Movie S2